HHS Public Access

Author manuscript

Mol Cell. Author manuscript; available in PMC 2020 October 03.

Published in final edited form as:

Mol Cell. 2019 October 03; 76(1): 11–26.e7. doi:10.1016/j.molcel.2019.06.043.

RAD51AP1 is an essential mediator of Alternative Lengthening of Telomeres

Jonathan Barroso Gonzalez[1], **Laura Garcia Exposito**[1], **Song My Hoang**[1], **Michelle Lee Lynskey**[1], **Justin L. Roncaioli**[1], **Arundhati Ghosh**[3], **Callen T. Wallace**[2], **Mauro Modesti**[4], **Kara A. Bernstein**[3], **Saumendra N. Sarkar**[3], **Simon C. Watkins**[2], **Roderick J. O'Sullivan**[1,*]

[1]Department of Pharmacology and Chemical Biology, UPMC Hillman Cancer Center, University of Pittsburgh, School of Medicine, Pittsburgh, Pennsylvania, USA

[2]Department of Cell Biology, UPMC Hillman Cancer Center, University of Pittsburgh, School of Medicine, Pittsburgh, Pennsylvania, USA

[3]Department of Microbiology and Molecular Genetics, UPMC Hillman Cancer Center, University of Pittsburgh, School of Medicine, Pittsburgh, Pennsylvania, USA

[4]Cancer Research Center of Marseille, CNRS UMR7258, Inserm UMR1068, Aix Marseille Université U105; Institut Paoli Calmettes, 27 Boulevard Lei Roure CS30059, 13273 Marseille, Cedex 09, France

SUMMARY

Alternative Lengthening of Telomeres (ALT) is a homology-directed repair (HDR) mechanism of telomere elongation that controls proliferation in aggressive cancers. We show that the disruption of RAD51-associated protein 1 (RAD51AP1) in ALT+ cancer cells leads to generational telomere shortening. This is due to RAD51AP1's involvement in RAD51 dependent homologous recombination (HR) and RAD52-POLD3 dependent break induced DNA synthesis. RAD51AP1 KO ALT+ cells exhibit telomere dysfunction and cytosolic telomeric DNA fragments that are sensed by cGAS. Intriguingly, they activate ULK1-ATG7 dependent autophagy as a survival mechanism to mitigate DNA damage and apoptosis. Importantly, RAD51AP1 protein levels are elevated in ALT+ cells due to MMS21 associated SUMOylation. Mutation of a single SUMO-targeted lysine residue perturbs telomere dynamics. These findings indicate that RAD51AP1 is an essential mediator of the ALT mechanism and is co-opted by post-translational mechanisms to maintain telomere length and ensure proliferation of ALT+ cancer cells.

[*]**Lead Contact:** Roderick J. O'Sullivan, osullivanr@upmc.edu.

AUTHOR CONTRIBUTIONS

J.B.G and R.J.O conceived and designed the study; J.B.G., L.G.E., conducted experimentation and analyzed the data. S.M.H., M.L.L., J.L.R. and R.J.O. assisted with experimentation and analyzed data. A.G. and S.N.M. provided assistance with assay development. C.T.W. and S.C.W. assisted with optical imaging experiment design and analyzes. K.A.B. and M.M. provided essential reagents and technical assistance. R.J.O. wrote the manuscript with assistance from J.B.G.

DECLARATIONS OF INTERESTS

The authors declare no competing interests.

Graphical Abstract

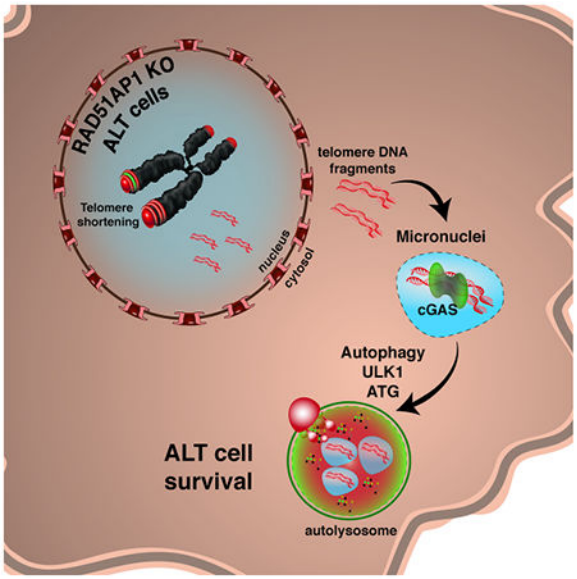

In Brief

Barosso-Gonzalez et al. identify that disruption of the HR accessory factor RAD51AP1 disrupts ALT telomere elongation causing telomere damage and fragmentation. Rather than dying, these cancer cells activate autophagy as a survival mechanism. The importance of RAD51AP1 in ALT cancer cells is underscored by its specific stabilization by SUMOylated mediated mechanisms.

Keywords

RAD51AP1; Telomere; Homology-Directed Repair; Autophagy; SUMOylation; Cancer

INTRODUCTION

An essential step in the acquisition of the cancer phenotype is the activation of a telomere elongation mechanism. Most cancer cells reactivate telomerase, a reverse transcriptase dedicated to the addition of telomeric TTAGGG repeat sequences at chromosome ends (Kim et al., 1994). However, when telomerase is suppressed, telomeres engage a homology directed repair (HDR) mechanism of telomere length maintenance termed Alternative Lengthening of Telomeres (ALT) (Bryan et al., 1997). Telomeres in ALT+ cells are intrinsically unstable and prone to replicative stress and spontaneous double strand break (DSB) formation that elicits recurrent activation of the DNA double strand break response (DSBR) (Cesare et al., 2009). These events provide the pro-recombinogenic stimuli for the two central HDR associated pathways that govern ALT telomere maintenance and extension. The first of these pathways involves RAD51 dependent homologous recombination (HR) between telomeres (Dunham et al., 2000). This is preceded by the assembly of the ssDNA-RAD51 presynaptic filament and homology search before the congression of multiple telomeres into large clusters, where it is presumed HR subsequently takes place (Cho et al.,

2014). This occurs primarily in S-phase as part of semi-conservative telomere replication. The second key step termed Break Induced Telomere DNA Synthesis (BITS) involves conservative synthesis of telomeric DNA sequences. Here, DSBs provoke the assembly of a non-canonical replisome consisting of PCNA-RFC-Polδ – of which POLD3 is essential for telomere extension (Dilley et al., 2016). RAD52 mediates mitotic DNA synthesis (MiDAS) and BITS during G2/M phase (Bhowmick et al., 2016; Sotiriou et al., 2016; Verma et al., 2019, Zhang et al., 2019). The ablation of these factors elicits strong anti-recombinogenic effects and perturbs telomere extension. It has also emerged that shifting the balance in favor of either HR or BITS through modulating the expression of HR factors such as BLM and SLX4 can have differential consequences on ALT telomere length - suggestive of need to co-regulate telomere replication and telomere extension in ALT cells (Sobinoff et al., 2017). Therefore, understanding how these pathways are functionally linked and deciphering which proteins are involved is a key unresolved issue.

RAD51AP1 is a vertebrate specific RAD51 interacting protein that stimulates RAD51 mediated homology search *in vitro* (Modesti et al., 2007; Wiese et al., 2007). RAD51AP1 exhibits a high affinity for structured DNA substrates *in vitro* and forms a stoichiometric interaction with UAF1 that enhances synapsis of paired homologous DNA strands and D-loop formation *in vitro* (Cukras et al., 2016; F. Liang et al., 2016). By virtue of its evident role(s) at the critical junctures of HR, we sought to determine whether RAD51AP1 participates in the ALT mechanism. We show that disruption of RAD51AP1 in ALT+ cells leads to progressive telomere shortening due to impaired HR and BITS and eventual dysfunction. The accumulation of cytosolic telomere DNA fragments activates cyclic GMP-AMP Synthase (cGAS) and AMPK-ULK1 dependent autophagic programs that sustain cellular survival of RAD51AP1 KO ALT+ cells. Finally, we discovered that RAD51AP1 protein levels are specifically elevated in ALT+ cancer cells. Biochemical studies reveal that this is due to MMS21 dependent SUMOylation of a single lysine within RAD51AP1, the mutation of which is sufficient to elicit telomere shortening in ALT+ cells. Cumulatively, these data reveal that RAD51AP1 is an essential mediator of the ALT mechanism.

RESULTS

RAD51AP1 disruption blocks ALT activity and leads to extensive telomere shortening

The association of RAD51AP1 with ALT telomeres was initially made in a proteomic analysis of telomere composition (García-Expósito et al., 2016). We confirmed the localization of endogenous RAD51AP1 to telomeres in several ALT+ cancer cell lines including U2OS and Saos2 (Figure 1A). This contrasted with the diffuse nucleoplasmic RAD51AP1 staining pattern observed in HeLa LT (Long Telomeres) and SJSA1 telomerase positive (TEL+) cells. RAD51AP1 was localized to ALT associated PML bodies (APBs) - specialized structures that are associated with telomere recombination in ALT+ cells (Figure 1A). Depleting RAD51AP1 by siRNA reduced the abundance of cells containing these APBs by ~50% (Figure 1B and S1A). An examination of metaphase chromosomes prepared from control and RAD51AP1 depleted U2OS cells by the COFISH assay revealed a reduction in telomeric sister chromatid exchanges (T-SCEs) and extra-chromosomal telomeric repeat (ECTR) DNA (Figure 1B). This reduction in ECTR was also confirmed in

U2OS and Saos2 ALT+ cells using the PCR based C-circle assay that quantitatively measures the abundance of C-rich circular telomeric DNA species (Figure S1A–B). Further analysis of metaphases chromosomes revealed evidence of enhanced telomere fragility, which correlates with incomplete telomere replication (Sfeir et al., 2009), in metaphases from RAD51AP1 depleted cells (Figure 1B and S1B). This indicated that depletion of RAD51AP1 diminishes ALT activity and suggested that long-term RAD51AP1 absence could impinge on telomere elongation.

RAD51AP1 gene expression was disrupted in U2OS ALT+ cells using CRISPR-Cas9 and several knock out (KO) clones were derived. After expansion in cell culture for ~25 population doublings (PDs), telomere length of control and validated RAD51AP1 knockout (KO) clones (*c1-c6*) was examined using pulsed field gel electrophoresis (PFGE) (Figure 1C). Unlike control U2OS clones whose bulk telomeres have a length ranging from 30 to 50kb, RAD51AP1 KO clones exhibited extensive telomere shortening to mean lengths of 25 to 30kb. The RAD51AP1 KO clones also exhibited reduced C-circle levels indicative of impaired ALT activity (Figure SIC). We noted that the intensity of the telomeric DNA smear was considerably weaker in lanes containing DNA from RAD51AP1 KO (Figure 1C). This could be due to stochastic telomere loss that was evident in metaphases derived from the control and RAD51AP1 KO clones (Figure S1D). Quantitative FISH (qFISH) analysis revealed that the distribution of telomere signal intensities in RAD51AP1 KO clones was narrower than in controls (Figure S1D). This is noteworthy as ALT telomere lengths are typically heterogeneous due to telomere recombination. Importantly, telomeres shortening with further culturing of the RAD51AP1 KO clones for~25PDs (Figure 1C). We calculated the generational telomere-shortening rate of the RAD51AP1 KO clones to be in the range of 100-600 base pairs/PD, which is greater than the shortening rate of 200bp observed in somatic cells lacking telomere length maintenance but could be accounted for by telomere loss. When GFP-tagged WT-RAD51AP1 was expressed in two of these KO clones (*c1 and c6*), the percentage of cells with APBs was restored to control levels (Figure 1D–E). Telomere shortening was attenuated and partially reversed in clones stably expressing GFP-WT -RAD51AP1 for ~20PDs (Figure 1F). ALT+ VA13 RAD51AP1 KO clones also exhibited significant telomere shortening over ~25PDs (Figure S1E) but telomerase positive (TEL+) HeLa LT RAD51AP1 KO clones did not (Figure S1F). These data show that RAD51AP1 is required for telomere length maintenance in ALT+ cancer cells, with its absence leading to telomere shortening like what is seen in cells lacking a functional telomere elongation mechanism.

RAD51AP1 regulates HR and POLD3 mediated DNA synthesis at ALT telomeres.

To determine how a deficiency of RAD51AP1 leads to profound effects on telomere length we asked if RAD51AP1 loss affected the key mechanistic steps of the ALT mechanism; HR and break induced telomere DNA synthesis (BITS). Prior to HR ALT telomeres initiate homology search within the nucleus and form large telomeric foci. This is dependent RAD51 and HOP2 proteins (Cho et al., 2014). We visualized and tracked telomere motion by live cell imaging using U2OS cells stably expressing eGFP-TRF1. After transfection with control and RAD51AP1 siRNAs the complete three-dimensional (x, y and z) mobility of eGFP-TRF1 foci was captured and telomere mobility was calculated as a function of mean

squared displacement (MSD). This analysis showed that the depletion of RAD51AP1 negatively impacted telomere motion in ALT+ cells - with a reduction in the cumulative MSD of telomeres from 16.93 μm^2 per hour in control cells to 13.4μm^2 per hour in RAD51AP1 knockdown cells (Figure S2A–B, Movie S1–2).

To pinpoint how the absence of RAD51AP1 impacts telomeres actively undergoing ALT mediated telomere extension, we took advantage of U2OS and VA13 cells expressing wildtype (WT) or catalytically inactive (DA) FokI endonuclease fused to TRF1. Here, cleavage of telomeric duplex DNA by WT-TRF1-FokI, but not DA-TRF1-FokI triggers RAD51 dependent homology search and clustering of telomeres into large foci that can be visualized and enumerated by immunofluorescence (Cho et al., 2014) (Figure 2A–B). The expected clustering of telomeres into larger foci and concomitant decrease in detectable telomeres was readily observed in WT-TRF1-FokI U2OS and VA13 cells transfected with control siRNAs. In contrast, the number of telomere clustering events was significantly reduced in RAD51AP1 depleted cells to levels observed when the catalytically inactive (DA) TRF1-FokI was used (Figure 2B). We concluded, therefore, that RAD51AP1 contributes to the spatiotemporal dynamics that precede ALT telomere elongation.

TRF1-FokI can also stimulate POLD3 dependent BITS (Dilley et al., 2016). Newly synthesized DNAs can be labeled with BrdU and subsequently recovered by immunoprecipitation with anti-BrdU antibodies. Using the same methodology and POLD3 knockdown as a control, we found that WT-TRF1-FokI induced nascent DNA synthesis was reduced by ~40% following depletion of RAD51AP1 (Figure 2C). Cumulatively, these data indicate that RAD51AP1 is one of the few proteins to be identified that contributes to each of the critical mechanistic steps of the ALT mechanism - providing a rationale for the extensive telomere shortening observed upon its disruption.

Impaired recruitment of POLD3 and RAD52 to telomeres in the absence of RAD51AP1

To better understand the dual actions of RAD51AP1 in regulating HR and BITS, we assessed its localization to telomeres during S and G2 cell cycle phases-when these critical steps are executed. RAD51AP1 localized equally to TRF1-FokI induced DSBs in S or G2 cell cycle phases, as inferred from a nuclear diffuse or focally enriched telomeric BrdU staining pattern (Figure 2D). In G2 cells, RAD51AP1 overlapped with BrdU foci at TRF1-FokI foci once again highlighting its close association with DNA synthesis activities at ALT telomeres. We confirmed that as with RAD51, RAD51AP1 co-localized with POLD3 and RAD52 at unperturbed telomeres and TRF1-FokI induced telomeric DSBs (Figure S2C). We then asked if the expression and recruitment of POLD3 and RAD52 is affected in the RAD51AP1 KO clones. The expression of RAD52 or POLD3 in RAD51AP1 clones was unchanged (Figure S2D). However, when WT-TRF1-FokI was transfected in the RAD51AP1 KO clones to induce the recruitment of these factors, we found that re-localization of RAD52 and, more significantly, POLD3 to TRF1-FokI foci was strongly impaired (Figure 2E).

It seemed that RAD51AP1 might interact with other HDR factors like POLD3 and/or RAD52. Indeed, transiently expressed GFP-RAD52 and FLAG-RAD51AP1 robustly co-immunoprecipitated (Figure 2F **and** S2E) independently of protein-DNA contacts as it

persisted following treatment with benzonase or ethidium bromide (Figure S2E). RAD52 forms foci in late S/G2 cells to mediate mitotic DNA Synthesis (MiDAS) (Bhowmick et al., 2016; Min et al., 2017; Özer et al., 2018; Sotiriou et al., 2016) and break induced telomere DNA synthesis (BITS) (Min et al., 2017; Özer et al., 2018; Verma:2019bv; Zhang:2019cn). Accordingly, we observed that the interaction between RAD52 and RAD51AP1 was equally robust when co-immunoprecipitated with extracts prepared from asynchronous and G2 arrested U2OS cells (Figure S2F). In mapping the interaction, we found that the C-terminal DMC1-RAD51 recombinase interaction module of RAD51AP1 *(lane 11)* and the conserved oligomerization domain of RAD52 *(lane 14)* are necessary for the interaction (Figure 2F,). Therefore, RAD51AP1 might co-regulate HDR by interactions with key regulators of HR (RAD51, PALB2) and BITS (RAD52) - rendering it uniquely positioned to integrate these two processes that are essential for the ALT mechanism.

Telomere dysfunction and fragmentation in RAD51AP1 KO ALT+ cells

Considering the apparent absence of ALT telomere elongation mechanism we wanted to monitor the fate of RAD51AP1 KO ALT+ cells. From ~25 population doublings (PDs) post single cell cloning, morphology changes and impaired colony formation proficiency were observed in U2OS RAD51AP1 KO clones (*c1-c6*). This was maintained over subsequent generations (Figure 3A **and** S3A). In somatic cells, telomere shortening and dysfunction leads to replicative senescence. However, this was not evident in the RAD51AP1 KO ALT+ cells. Only two clones (*c3* and *c5*) exhibited a modest increase in senescence associated β-galactosidase activity (SAbG) (Figure S3B). However, protein analysis revealed that each clone harbored elevated DNA damage signaling with robust phosphorylation of serine 1981 (S1981) of Ataxia Telangiectasia Mutated (ATM), serine 139 (S139) of histone H2AX and threonine 68 (T68) of Checkpoint Kinase 2 (CHK2) (Figure 3B). The RAD51AP1 KO U2OS clones exhibited genomic instability with a greater number of defective mitoses with more unaligned and lagging chromosomes (Figure S3C). Proliferative delay and histone H2AX phosphorylation were also observed in VA13 RAD51AP1 KO clones, whereas proliferation of RAD51AP1 KO HeLa LT was relatively unperturbed (Figure S3D–E). There was an accumulation of 53BP1 DNA damage foci at telomeres, also termed telomere dysfunction induced foci (TIFs), and more frequent micronuclei (Figure 3C–D). Fragments of damaged DNA, including those derived from damaged genomic DNA and telomeres, that are expunged into the cytoplasm during mitosis can be sensed by cyclic GMP-AMP Synthase (cGAS) (Harding et al., 2017; Mackenzie et al., 2017; Nassour et al., 2019). IF-FISH revealed a significant increase in cGAS positive micronuclei in the U2OS and VA13 RAD51AP1 KO clones, a large proportion of which harbored telomeric DNA (Figure 3D **and** Figure S3F). The DNA damage signaling, accumulation of TIFs and cGAS positive micronuclei was attenuated or reduced in clones re-expressing WT-RAD51AP1 (Figure S4A–B). Thus, absence of RAD51AP1 protein leads to telomere shortening and dysfunction that eventually potentiates fragmentation and expulsion of telomeric DNAs into the cytosol, where they are sensed by cGAS.

Activation of autophagy in RAD51AP1 KO ALT+ cells.

As with cellular senescence, we did not detect the apoptosis associated cleavage of Poly ADP-Ribose Polymerase 1 (PARP1) or Caspase-3 in RAD51AP1 KO protein extracts

(Figure 3E). Micronuclei that form due to oncogenic stress or DNA damage can activate autophagy to eliminate aberrant DNA species and damaged organelles (Dou et al., 2015; Rello-Varona et al., 2012). Recently, catastrophic telomere dysfunction accompanied by cGAS mediated sensing of micronuclei associated telomeric DNA species elicited autophagic cell death during replicative crisis was described (Nassour et al., 2019). Indeed, the cytoplasmic vacuolization that is characteristic of autophagy was observed in the RAD51AP1 KOs suggesting autophagy might also be active (Movie S3). In agreement with this, RAD51AP1 KO U2OS clones clearly exhibited an accumulation of light chain 3 protein A (LC3A) and processing to its lipidated B-form (LC3B) that is essential for autophagosome biogenesis. There was also a modest increase of lysosomal-associated membrane protein 1 (LAMP1) and degradation of the autophagy receptor protein p62 (SQSTM1) that correlate with autolysosome maturation and autophagic flux, respectively (Levine and Kroemer, 2019)(Figure 3E). Importantly, p62 protein levels were reversed to normal levels with the autophagy flux inhibitor, bafilomycin A1 (Figure 3E).

To confirm the activation of autophagic flux and autolysosome biogenesis, we utilized a tandem mCherry-GFP tagged LC3B pH-based autophagy reporter system. The acidification of double positive mCherry/GFP (yellow) LC3 within mature autolysosomes quenches GFP signal leaving only detectable mCherry positive (red) active autolysosomes (N'Diaye et al., 2009). This provides a qualitative and quantitative readout of autolysosome maturation and autophagic flux. In the U2OS RAD51AP1 clones a robust increase in the percentage of cells harboring red LC3 puncta was observed and reversed by bafilomycin A1 (Figure 3F). A similar effect was observed in two of the three VA13 RAD51AP1 KO clones (Figure S4C). Importantly, LC3 levels were also reduced in U2OS RAD51AP1 KO clones expressing WT-RAD51AP1 that exhibited reduced levels of DNA damage and micronuclei (Figure S4A–B). This indicates that it is the absence of RAD51AP1 and accumulation of dysfunctional, fragmented telomeres that provides the impetus for autophagy activation. It is also consistent with evidence that telomere damage is a potent and specific activator of autophagic programs (Nassour et al., 2019.

ULK1 dependent autophagy promotes survival of RAD51AP1 KO ALT+ cells.

Autophagy usually acts a cytoprotective mechanism to remove damaged proteins and organelles and recycle metabolites that sustain cellular viability (Levine and Kroemer, 2019). During basal conditions the pro-autophagic activity of ULK1 kinase is constrained through inactivating phosphorylation at serine 757 (S757) by the mechanistic target of rapamycin complex 1 (TORC1). Activation of AMP activated protein kinase (AMPK) by phosphorylation at threonine 172 (T172) within the a subunit, promotes phosphorylation of ULK1 at serine 555 (ULK1-S555) (Egan et al., 2011) that overrides TORC1 inhibition of ULK1. Active ULK1 then phosphorylates its downstream targets of which Beclin1 serine 15 (S15) is one of the most important for autophagy initiation. Accordingly, we detected increased phosphorylation of AMPKα-T172, ULK1-S555 and Beclin1-S15 in RAD51AP1 KO cells (Figure 4A). Phosphorylation at S757 in ULK1, which is the target for TORC1, was not altered. Furthermore, treatment of control and RAD51AP1 KO cells with SBI-0206965, a selective inhibitor of ULK1-S555 phosphorylation (Egan et al., 2015), reduced phosphorylation of ULK1-S555, AMPKα-T172 and Beclin 1-S15 (Figure 4A).

ULK1 inhibition blocked processing of LC3B and restored p62 protein to normal levels (Figure 4A). Autolysosome maturation and flux was also impaired as shown by a reversion from red to yellow puncta using the GFP-mCherry-LC3B reporter (Figure S4D). Therefore, the autophagy observed in the RAD51AP1 KO clones appeared to be mediated by the AMPK-ULK1 pathway.

The cGAS-STING axis has a key role in activating an alternative autophagy pathway to respond to the presence of cytosolic genomic and viral DNA (Gui et al., 2019). This pathway is stimulated by 2, 3 cGAMP produced by cGAS followed by translocation and degradation of STING through the Endoplasmic-Reticulum/Golgi Intermediate Compartment (ERGIC) (Gui et al., 2019). This does not rely on ULK1 and Beclin1 or stimulation of interferon by STING and TBK1 (Gui et al., 2019). Both cGAS and STING are essential for the induction of autophagic cell death observed during replicative crisis of human mammary epithelial cells (HMECs) and primary fibroblasts (Nassour et al., 2019). However, STING expression is often barely detectable in cancer cell lines and is inactivated in ALT+ cells (Chen et al., 2017). Therefore, it was not likely that the alternative cGAS-STING dependent autophagy pathway is active in the RAD51AP1 KO ALT+ cells. cGAS on the other hand is expressed and active in ALT+ cells (Figure 3D) (Harding et al., 2017; Mackenzie et al., 2017) and can crosstalk with the conventional autophagy pathway through an interaction with Beclin1 and stimulates ULK1 activity (Konno et al., 2013; Q. Liang et al., 2014).

To determine the consequences of AMPK-ULK1 mediated autophagy, we depleted ULK1 and core autophagy proteins ATG5 and ATG7 that are essential for autophagosome biogenesis and maturation, as well as cGAS in U2OS and VA13 ALT+ cells. Knockdown was confirmed by western blot and cell growth was assessed by clonogenic assay (Figure 4B). U2OS and VA13 RAD51AP1 KO clones depleted of cGAS, ULK1 or ATG7 exhibited strong growth attenuation - with some near completely eliminated (Figure 4C–D **and** Figure S4E–F). We confirmed using the mCherry-GFP tagged LC3B reporter that autolysosome biogenesis was impaired in ULK1 and ATG7 depleted cells and to a lesser, though significant, extent in those lacking cGAS (Figure 4E). Protein analysis revealed that p62 degradation was reversed after depletion of ULK1 and ATG7, and the processing of LC3A to LC3B also appeared affected. Importantly, the remaining ULK1 and ATG7 depleted RAD51AP1 KO cells displayed markedly elevated histone H2AX phosphorylation and cleavage of Caspase-3, a marker of commitment to apoptosis (Figure 4F). This was confirmed in flow cytometry which revealed an ~2-4 fold increase in the percentage of cells that stained positive for cleaved caspase-3 (Figure 4D and S4F). Throughout, we found that depletion of ATG5 did not alter cell survival or promote caspase activation (Figure 4C–D) or autophagic signaling (i.e. p62 degradation/LC3B processing) (data not shown) indicating that it is dispensable for autophagy in this context. The basis for this might be ATG5-12's greater role in LC3 lipidation during cGAS-STING mediated autophagy, as was described (Gui et al., 2019). We also noticed that the survival and basal level of autolysosomes present in control U2OS and VA13 cells was affected by the depletion of ULK1 and ATG7 suggesting that autophagy be necessary for ALT+ cell survival (see discussion)(Figure 4C–D). Collectively, these data demonstrate that the AMPK-ULK1 autophagy pathway

promotes survival of RAD51AP1 KO ALT+ cancer cells that exhibit telomere shortening and dysfunction when ALT telomere maintenance is perturbed.

RAD51AP1 protein is stabilized in ALT+ cancer cells.

The data pointed to RAD51AP1 having a particular importance in mediating telomere maintenance and survival of ALT+ cancer cells. Therefore, it was significant that the levels of RAD51AP1 protein were elevated in ALT+ cell lines, as opposed to primary and TEL+ cancer cell lines (Figure 5A **and** S5A). This was not due to increased transcription of its mRNA (data not shown) implicating post-translational mechanisms. By performing cycloheximide (CHX) chase experiments we determined that in comparison to other key ALT associated proteins (RAD51, POLD3, RAD52) RAD51AP1 protein is roughly twice as stable in a panel of ALT+ cells (Mean $t_{1/2}$=10.4hrs) compared with TEL+ cells (Mean $t_{1/2}$=4.6hrs) (Figure 5B). The stability of RAD51AP1 was enhanced when TEL+ cells (HeLa LT) were exposed to the DNA damaging agent etoposide (Figure S5B). RAD51AP1 stability was independently assessed in U2OS, VA13 (ALT+) and HeLa LT, SJSA1 (TEL+) cells by pulse labeling of newly synthesized proteins with ^{35}S-methionine and cysteine and harvesting of cells at 4hr intervals during a chase with unlabeled amino acids. This revealed that, as was the case with CHX experiments, that RAD51AP1 is significantly more stable in ALT+ ($t_{1/2}$ = 7.1hrs, +/− 1.4hrs) compared with TEL+ cell lines ($t_{1/2}$ = 4.6hrs, +/− 0.9hrs) (Figure S5C–D). It seems plausible that the intrinsic instability and chronic DNA damage of ALT telomeres promotes the stabilization of RAD51AP1 allowing it to act during HR and DNA synthesis steps of the ALT mechanism.

MMS21 mediated SUMOylation and stabilization of RAD51AP1.

RAD51AP1 protein contains a intrinsically disordered region (IDR) that extends from the N-terminal PALB2 domain *(aa120),* through the central portion to the C-terminal DMC1-RAD51 *(aa283-352)* interaction module (Figure 5C). These have been intensely studied due to their capacity to foster transient and reversible protein-protein interactions particularly those involving SUMO (small ubiquitin like modifier) (Hendriks et al., 2017). SUMOylation of RAD51AP1 has been identified in proteomic studies of DNA damage induced SUMOylation (Hendriks et al., 2017; Lamoliatte et al., 2017). Furthermore, RAD51AP1 contains a SUMO-Interacting Motif (SIM) domain *(aa137-140)* that is required to mediate synaptic complex and D-loop assembly, through direct binding with UAF1 (Cukras et al., 2016; F. Liang et al., 2016).

We verified that RAD51AP1 could be poly-SUMOylated by immunoprecipitation of endogenous RAD51AP1 from U2OS cells expressing HA tagged WT-SUMO-2/3 (Figure S6A). Overexpression of SUMO protein and immunoprecipitations of the target proteins are necessary because only a small pool of any given protein is typically modified. To control for SUMO overexpression we also expressed mutant HA-ΔGG-SUMO-2/3 that lacks the terminal glycines necessary for SUMO conjugation and could not detect SUMO in the RAD51AP1 IP. We also confirmed previous reports of RAD51AP1 ubiquitination (Cukras et al., 2016) in U2OS cells expressing HA-WT-Ubiquitin, but not mutant HA-ΔGG-Ubiquitin that similarly lack the C-terminal glycines necessary for ubiquitin conjugation (Figure S6A). Interestingly, RAD51AP1 SUMOylation could be stimulated following expression and

induction of telomeric damage with WT-TRFl-FokI and by global DNA damage induced by etoposide (Figure S6B). Furthermore, RAD51AP1 SUMOylation was found to be equal in co-IPs performed with extracts prepared from synchronous and G2 synchronized U2OS HA-SUMO cells (Figure S6C). To determine whether RAD51AP1 is directly SUMOylated, we expressed tagged RAD51AP1 in HA-SUMO2 U2OS cells and performed reciprocal immunoprecipitations using HA or GFP antibodies. In each case, GFP-RAD51AP1 and discrete bands corresponding to mono, di, tri etc and polySUMOylated RAD51AP1 were detected providing strong evidence for its SUMOylation (Figure S6D).

The SUMO E3 ligase MMS21 has been implicated in telomere maintenance by ALT (Potts and Yu, 2007). To assess whether MMS21 modifies RAD51AP1, we performed an *in vivo* SUMOylation assay. When FLAG-RAD51AP1 was expressed and immunoprecipitated from HA-SUMO U2OS cells, higher molecular bands consistent with SUMO-RAD51AP1 conjugates could be detected at high exposure directly in FLAG western. The intensity of these bands was enhanced when WT-MMS21, but not the ligase dead MMS21 mutant (CA) was co-expressed with FLAG-RAD51AP1, indicative of its SUMOylation by MMS21 (Figure S6E). Accordingly, WT-MMS21, but not the ligase-dead mutant of MMS21 (C215A), stimulated poly-SUMOylation of FLAG-tagged RAD51AP1 (Figure 5C). Interestingly, we found that GFP-WT-MMS21 and FLAG-RAD51AP1 interacted in co-IP (Figure S6F). The association seemed greater when the ligase dead MMS21 was expressed suggesting a dynamic interaction. That MMS21 binds RAD51AP1 is consistent with the model where E3 ligases directly interact with substrates enabling them to receive SUMO *in cis* from adjacent SIMs and modify their target lysines (Gareau and Lima, 2010). We next examined how depletion of MMS21 would affect RAD51AP1 SUMOylation (Figure 5D **and** S6G). MMS21 knockdown strongly reduced RAD51AP1 SUMOylation. As a control, depletion of UBC9 - preventing all SUMO conjugation - yielded a similar reduction suggesting that the bulk, if not all of the SUMOylation of RAD51AP1 depends on MMS21. Knockdown of SENP6, a protease that deSUMOylates proteins, modestly increased RAD51AP1 SUMOylation (Figure 5D **and** S6G). The results of these experiments strongly supported the likelihood that MMS21 is responsible for RAD51AP1 SUMOylation.

In silico analysis of RAD51AP1 protein sequence identified four lysine residues (K44, K240, K269, K326) embedded within strong SUMO consensus sequences ψKxD/E (where ψ is a large hydrophobic residue, and X is any residue) (Figure 5E). To identify which residue(s) of RAD51AP1 are SUMOylated, we generated a series of lysine-arginine mutations in the four predicted SUMO sites in myc-tagged RAD51AP1 for expression in HA-SUMO U2OS cells. This analysis revealed that mutation of lysine 269 (K269), located within the C-terminal portion of RAD51AP1s IDR, greatly reduced the SUMOylation of myc-tagged RAD51AP1 (Figure 5E). Mutating the SIM domain (L137A, I140A, V142A) (F. Liang et al., 2016) also reduced RAD51AP1 SUMOylation likely due to its requirement in binding the SUMO E2-conjugase, UBC9, which typically interacts with E3 ligases that mediates site-specific modification of protein substrates (Gareau and Lima, 2010). In these experiments, we observed opposing patterns of SUMO and ubiquitin modification of RAD51AP1. Overexpression of MMS21 increased SUMOylation and reduced ubiquitination of RAD51AP1 (Figure 5C). This contrasted with the effect of MMS21

depletion that while reducing SUMOylation significantly enhanced the ubiquitination of the protein (Figure 5D). RAD51AP1 ubiquitination was almost entirely abolished in the K269R mutant and strongly reduced in the ΔSIM mutant (Figure 5E). When the stability of SUMO/Ubiquitin defective K269R and ΔSIM RAD51AP1 was examined by CHX-western we found that both were considerably more stable compared to WT-RAD51AP1 (Figure 5F). Notably, knockdown of MMS21 and UBC9 significantly destabilized RAD51AP1, enhancing its turnover. This indicated that SUMO and Ubiquitin E3 ligases competitively modify the same lysine residue (K269) of RAD51AP1 and that SUMOylation sequesters RAD51AP1, protecting it from ubiquitination that marks it for degradation.

SUMOylation of RAD51AP1 is necessary for ALT telomere elongation.

Having established that SUMOylation stabilizes RAD51AP1 in ALT+ cells we wanted to examine its functional relevance. As with WT-RAD51AP1, we found that both GFP-tagged K269R and ΔSIM-RAD51AP1 localized to telomeres in U2OS cells - ruling out an involvement for SUMO in its localization (Figure S7A–B). Consistent with RAD51AP1s requirement to bind RAD51, a mutant lacking the RAD51 and PALB2 interacting domains was delocalized from telomeric foci (Figure S7A–B). Also, depletion of RAD51, MRE11 and CtIP abolished RAD51AP1s association with telomeres (Figure S7C). RAD51AP1 SUMOylation was reduced when RPA1, MRE11-CtIP and to a lesser degree RAD51 were depleted (Figure S7D). Therefore, RAD51AP1 SUMOylation seems coupled to DNA resection and downstream activities in HDR. We tested whether re-expression of SUMO-defective RAD51AP1 mutants could rescue the deficiencies in APB formation and ALT telomere dynamics twhen RAD51AP1 is depleted (Figure 6A–B). Unlike WT-RAD51AP1, neither K269R nor ΔSIM-RAD51AP1 could fully restore APBs levels (Figure 6B left). This failure to compensate was more pronounced in WT-TRF1-FokI induced telomere-clustering experiments (Figure 6B **right**). Here, SUMO-defective RAD51AP1 mutants performed as poorly as the ΔRAD51 mutant protein implying that SUMOylation of K269 in RAD51AP1 is by itself required for appropriate telomere clustering in ALT+ cells.

We examined if SUMO defective RAD51AP1 could attenuate and stabilize telomere length, as the WT-RAD51AP1 did, when expressed in RAD51AP1 KO clones *(cl and c6).* Cells expressing equal levels of GFP-tagged WT, K269R or ΔSIM-RAD51AP1 (Figure 6C) were seeded and their proliferation was first assessed by colony formation assays. This revealed that, as before, WT-RAD51AP1 significantly ameliorated the proliferative defects of RAD51AP KO clones *(cl and c6),* neither of the SUMO-defective mutants could (Figure 6D). When telomere length was analyzed, we observed that K269R or ΔSIM RAD51AP1 could not fully rescue the telomere length defects observed in the RAD51AP1 KO clones as efficiently as WT-RAD51AP1 (Figure 6E). This was most apparent with the K269R mutant suggesting that SUMOylation through this site is very important for telomere maintenance in ALT+ cells. We also stably expressed WT, K269R or ΔSIM RAD51AP1 in cells expressing endogenous RAD51AP1 - with the idea that co-existence of WT and SUMO defective RAD51AP1 could have dominant negative effects on telomere length. In stark contrast with cells expressing WT-RAD51AP1 which modestly increased in telomere length, stable expression of K269R or ΔSIM RAD51AP1 resulted in significant telomere shortening to lengths of ~23kb (Figure 6F). This suggests that the stabilization of RAD51AP1

conferred by SUMOylation is a critically important aspect of sustaining the ALT mechanism - particularly it seems with respect to telomere congression during HR and telomere length.

DISCUSSION

We identified a key role for the vertebrate specific HR accessory protein RAD51AP1 in regulating the ALT mechanism. RAD51AP1 disruption in ALT+ cells leads to extensive and sustained telomere shortening. By definition, this result implies that the ALT mechanism is inhibited when RAD51AP1 protein is absent. To date, few proteins have been shown to contribute to both critical steps of the ALT mechanism; RAD51 dependent HR and RAD52-POLD3 mediated BITS. The essential role of RAD51AP1 on ALT telomere maintenance and extension are certainly unexpected, considering the relatively modest effects of its perturbation during HR mediated repair of DSBs (Wiese et al., 2007; F. Liang et al., 2016). The affinity of RAD51AP1 for D-loops, a common factor and key platform for DNA/protein transactions within HR and BITS, could bring it into proximity with the essential mediators of the ALT mechanism during these key stages. Its stabilization by SUMOylation may confer on RAD51AP1 a specific capacity to regulate the ALT mechanism. While several precise details remain to be determined - RAD51AP1 joins a short list of proteins that regulate multiple aspects of the ALT mechanism.

Fine tuning of ALT by RAD51AP1 SUMOylation

While mutants within the SUMO pathway display strong phenotypes, the disruption of single SUMOylation sites rarely shows any effect (Geiss-Friedlander and Melchior, 2007). The SUMOylation of RAD51AP1 is striking for its strong phenotypic effects on telomere dynamics and length. There is considerable evidence that SUMOylation events in the context of DNA repair are functionally integrated, with some individual modifications having greater influence over others (Jackson and Durocher, 2013; Psakhye and Jentsch, 2012). Following DNA damage, SUMO modifications can foster synergistic interactions by attracting SUMO-interaction motif (SIM) containing HDR proteins that bind promiscuously to available SUMOylated residues (Psakhye and Jentsch, 2012). These can include SIM containing SUMO E3 ligases (e.g. PIAS1-4) that amplify the SUMO modification signal or multi-SIM containing proteins that potentiate protein complex assembly through multiple homo and heterotypic interactions (Galanty et al., 2009; Guervilly et al., 2015; Yang et al., 2011). The high concentrations of SUMO-SIM interactions can alter the electrostatic properties of the sub-nuclear locale - as exemplified by the ability of SUMO-SIM interactions to form liquid droplets by phase separation (Banani et al., 2016). That RAD51AP1 is structurally disordered could be significant since such proteins have emerged as important conduits of adaptive structural configurations in response to DNA damage - including as mediators of phase separation. Aside from its known interaction with RAD51 and RAD52, that we described here, we expect other proximal interactors of RAD51AP1 are coregulated by SUMOylation during ALT. While there is strong evidence that SUMOylation is an important feature of ALT (Potts and Yu, 2007), deciphering and understanding how individually modified proteins such as RAD51AP1 operate and interact within the greater SUMO regulated protein network could provide important insights of SUMOylation in regulating the ALT mechanism.

Perturbation of ALT telomere elongation accentuates cytoprotective autophagy

During replicative crisis, cells are faced with potential catastrophic effects wrought by telomere fusions that can elicit complex genome rearrangements. At this time, pre-malignant cells are systemically eliminated by autophagic death. This discovery established autophagy as an essential tumor suppressive mechanism (Nassour et al., 2019). In cells lacking ALT telomere maintenance, we observed the release of fragments of telomeric DNAs into the cytosol that are sensed by cGAS and likely removed by autophagy. This is mediated through AMPK-ULK1 and ATG7 mediated autophagosome biogenesis and blocking autophagy activated apoptotic cell death programs, virtually eliminating the RAD51AP1 KO cells. Therefore, in this context, autophagy acts as a survival mechanism to mitigate detrimental events arising from recurrent telomere dysfunction and to perhaps recycle cellular metabolites.

We also observed that the viability of control ALT+ cancer cells (U2OS and VA13) was affected by depletion of ULK1 and ATG7 proteins suggesting that they harbor a more pronounced basal level of autophagy. We interpreted this as implying that following escape from crisis, and achieving full transformation ALT+ cancer cells adapt and utilize autophagy as a chronic survival mechanism to offset the threat posed by the recurrent instability of telomeres. Yet, when telomere shortening and dysfunction reaches critical levels as in the RAD51AP1 KO ALT+ cancer cells, this is amplified, through elevated cGAS signaling that enhances the AMPK-ULK1 pathway and clearance of damaged cells by autophagy. Thus, as envisioned by Nassour et al., and further developed here, the inhibition of autophagy as a cancer therapy could represent a double edged sword - proving catastrophic in the context of cancer initiation yet perhaps beneficial once cellular transformation has developed past this critical window and ALT telomere maintenance is activated. Finally, it has been reported that cells with defective autophagy fail to activate compensatory DNA repair pathways including HR and NHEJ following exposure to DNA damaging agents (Hewitt and Korolchuk, 2017). These studies suggested the possibility of a synthetic lethal interaction between autophagy and DNA repair pathway inhibition. Since RAD51AP1 KO cells are defective in HDR and clearly more sensitive to autophagy inhibition, this is in line with this expectation. Given the reliance of ALT cancer cells on DNA repair mechanisms as default means of sustaining their proliferation, the combined inhibition of autophagy and HDR might hold promise for ALT+ cancer cell therapy.

STAR★METHODS

Detailed methods are provided in the online version of this paper and include the following:

CONTACT FOR REAGENT AND RESOURCE SHARING

Further inquiries and requests for resources and reagents should be directed to and will be fulfilled by the Lead Contact, Roderick J. O'Sullivan (osullivanr@upmc.edu).

DATA AND SOFTWARE AVAILIBILITY.

Raw data files, images and immunoblots were deposited on Mendeley and are available at : http://dx.doi.org/10.17632/7frzkkgz74.1

EXPERIMENTAL MODEL AND SUBJECT DETAILS

Cell Culture—All cell lines were obtained from ATCC. Each cell line was cultured in Glutamax-DMEM (Life Technologies) supplemented with 10% bovine growth serum. Cells were cultured at low oxygen conditions of 3% O_2 and 7.5% CO_2. U2OS and HeLa LT cell lines were authenticated by STR profiling and confirmed mycoplasma free by ATCC cell line authentication services. To generate the U2OS cell lines stably expressing HA-Ubiquitin, HA-SUMO3 or tagged RAD51AP1, cells were transfected with either HA-SUMO3 or ΔGG mutant, HA-Ubiquitin or ΔGG mutant, GFP alone or GFP-RAD51AP1 expression plasmids in 6cm plates. 48hrs after transfection, cells were transferred to 10cm plates and selected with 500μg/mL G418 every two days for one week. Stable expression of the transgene was tested by western blot using an HRP-conjugated HA or GFP antibodies. U2OS myc-RAD51AP1 WT, K269R and DSIM cell lines were generated by retroviral transduction as previously described (Garcia-Exposito L. et al. 2016). Briefly, pLPC-based retrovirus were produced in 293FT cells by co-transfecting pLPC-RAD51AP1 constructs together with pMD.G (VSV-G expressing plasmid). 48hrs after transfection, filtered supernatants were used to infect U2OS cells. Stable cells were selected with 2μg/mL puromycin for ~1 week. Stable expression of the myc-tagged transgene was analyzed by western blot. pLKO-based lentivirus were produced in 293FT cells by co-transfecting pLKO constructs containing either control or shRNAs against cGAS, ATG7, ATG5 or ULK1 together with psPAX2 and pMD2.G packing plasmids to produce lentivirus. 48hrs after transfection, filtered supernatants were used to infect U2OS cells. Protein knockdown was analyzed by western blot after 1 week of infection.

Generation of RAD51AP1 KO cells by CRISPR/Cas9.—LentiCRISPR v2 plasmids containing RAD51AP1 sgRNAs were transfected with Lipofectamine 2000 (Life Technologies) into 293FT cells along with psPAX2 and pMD2.G packing plasmids to produce lentivirus. Media was change 16hrs after transfection and virus were harvested and filtered ~48hrs after media change and stored at −80 °C or used to infect U2OS, HeLa LT or VA13 cells for 2 days. Then, cells were selected with 2μg/mL puromycin for 1 week before performing single cell sorting in 96 wells to isolate individual clones. Clones were tested by western blot for the absence of RAD51AP1 protein staining. To rescue RAD51AP1 in CRISPR cells, an eGFP-tagged RAD51AP1 construct resistant to Cas9 cleavage, generated by site-directed mutagenesis of the PAM sequence, was transfected in RAD51AP1 KO CRISPR clones. ~48hrs after transfection, cells were selected with 500μg/mL G418 every two days for two weeks. Then, eGFP-positive cells were sorted by flow cytometer and expression was tested by IF and western blot. As a parallel control, same RAD51AP1 CRISPR clones were stably transfected with a GFP protein expressed form the same vector backbone.

METHOD DETAILS

Colony Formation Assays—1000 HeLa LT, U2OS or 5000 VA13 cells were seeded in 6 well plates in triplicate and cultured for 7 days before fixation and staining in a 1% crystal violet solution. Plates were images and analyzed with Protein Simple FluorChem system, which was used to count positive stained colonies and calculate total cell coverage per well. For experiments involving shRNAs, control and RAD51AP1 KO clones (c1-c6) cells were

infected with lentivirus expressing shRNAs control or targeting ATG5, ATG7, ULK1 or cGAS. After two days of infection, culture media was replaced and cells were counted after another 7 days for colony formation assay as described.

Telomere Restriction Fragment analysis by Pulsed Field Gel Electrophoresis.—Telomere gels were performed using telomere restriction fragment (TRF) analysis. Genomic DNA was digested using *AluI* and *MboI* (NEB). 4-10 μg of DNA was run on a 1% PFGE agarose gel (Bio-Rad) in 0.5×TBE buffer using the CHEF-DRII system (Bio-Rad) at 6V cm-1; initial switch time 1 second, final switch time 6 seconds, for 17hrs at 14°C. The gel was then dried for 2hrs at 60°C, denatured in a 0.5 N NaOH 1.5 M NaCl solution, and neutralized. Gel was hybridized with ^{32}P-labelled $(TTAGGG)_4$ oligonucleotides in Church buffer overnight at 55°C. The next day, the membrane was washed three times in 2×SSC buffer and once in 2x SSC 0.5% SDS, exposed onto a storage phosphor screen and scanned using Typhoon 9400 Phospholmager (GE Healthcare). Telomere length was determined using TeloTool software.

C-Circle Assay.—CC assay was performed as described (Henson et al., 2009). Genomic DNA was purified, digested with *AluI* and *MboI* and cleaned up by phenol-chloroform extraction and precipitation. DNA was diluted in ultraclean water and concentrations were exhaustively measured to the indicated quantity (generally, 30, 15 and 7.5ng) using a Nanodrop (ThermoFisher). Samples (10 μl) were combined with 10μl BSA (NEB; 0.2 mg/ml), 0.1 % Tween, 0.2 mM each dATP, dGTP, dTTP and 1χ Φ29 Buffer (NEB) in the presence or absence of 7.5U ΦDNA polymerase (NEB). Samples were incubated at 30°C for 8hrs and then at 65°C for 20mins. Reaction products were diluted to 100μl with 2^XSSC and dot-blotted onto a 2^xSSC-soaked nylon membrane. DNA was UV cross-linked onto the membrane and hybridized with a P_{32} end-labelled $(CCCTAA)_4$ oligo probe to detect C-circle amplification products. All blots were washed, exposed to Phospholmager screens, scanned using a Typhoon 9400 Phospholmager (GE Healthcare) and quantified with Image J. In all reactions, when Φ29 was omitted as a negative control DNA was used.

Immunoprecipitations.—U2OS stably expressing myc, myc-RAD51AP1 WT, myc-RAD51AP1-K269R or myc-RAD51AP1-ΔSIM were transiently transfected with either SUMO3-HA or Ubiquitin-HA for 24 hrs. Then, myc-tagged proteins were immunoprecipitated using μMACS c-myc epitope tag Isolation Kit (Miltenyi Biotech) according to manufacturer's instructions. The fraction of myc-tagged constructs modified by SUMO3 or Ubiquitin were detected using an HRP-conjugated HA antibody. To study endogenous RAD51AP1 modification by SUMO3 WT, SUMO3 ΔGG, Ubiquitin WT or Ubiquitin ΔGG, U2OS stably expressing HA-tagged SUMO3 or Ubiquitin either WT or mutant proteins were harvested in 50 mM Tris-HCl (pH 7.5), 150 mM NaCl, 1% NP-40 containing protease inhibitors and 20mM N-ethylmaleimide. Endogenous RAD51AP1 was specifically immunoprecipitated, and the RAD51AP1 fraction modified by SUMO3 or Ubiquitin was detected using an HRP-conjugated HA antibody. To study endogenous RAD51AP1 modification by SUMO3 or Ubiquitin in siRNA knockdown cells, U2OS stably expressing SUMO3-HA or Ubiquitin-HA were transfected with a control siRNA or siRNAs as indicated. ~72hrs after siRNA, cells were harvested as described above. Then,

endogenous RAD51AP1 was specifically immunoprecipitated and the RAD51AP1 fraction modified by SUMO3 or Ubiquitin was detected using an HRP-conjugated HA antibody. To study MMS21-mediated RAD51AP1 modification by SUMO3 or Ubiquitin, U2OS stably expressing HA-tagged SUMO3 or Ubiquitin either WT or ΔGG mutants were transfected with 3xFLAG-RAD51AP1 together with GFP alone, GFP-MMS21 WT or GFP-MMS21 CA mutant for 24hrs before their harvest and lysis as described above. Cleared lysates were used for immunoprecipitation using FLAG-M2 agarose beads (Sigma) and the RAD51AP1 fraction modified by SUMO3 or Ubiquitin was detected using an HRP-conjugated HA antibody. To study RAD51AP1 modification by SUMO3 using reverse immunoprecipitation, U2OS stably expressing HA-tagged SUMO3 were transfected with GFP alone or GFP-RAD51AP1 for 24hrs before their harvest and lysis as described above. Cleared lysates were split in two and used for immunoprecipitation using either GFP or HA μMACS epitope tag Isolation Kit (Miltenyi Biotech) according to manufacturer's instructions. The fraction of GFP-tagged constructs modified by SUMO3 was detected using an HRP-conjugated HA antibody, and the fraction of GFP-tagged construct present in total SUMO3 conjugates was detected using an HRP-conjugated GFP antibody. For co-immunoprecipitation experiments, U2OS were transiently transfected with either 3xFLAG-tagged RAD51AP1 together with GFP-tagged RAD52 for 24hrs before their harvest and lysis as described above. Cleared lysates were used for immunoprecipitation using FLAG-M2 agarose beads (Sigma) and co-immunoprecipitated RAD52 was detected by western blot using a GFP antibody. When indicated, cells were pre-incubated with the CDK1 inhibitor RO-3306 (10μM) for 20hrs before cell lysis. To investigate DNA dependency on interactions, immunoprecipitations were performed in the presence of 20μg/ml ethidium bromide (Invitrogen) or 100 units of Benzonase (Thermo Scientific).

Western Blotting.—Cells were harvested with trypsin, quickly washed in PBS, counted with Cellometer Auto T4 (Nexcelom Bioscience) and directly lysed in 4X NuPage LDS sample buffer at 10^4 cells per μl. Proteins were gently homogenized using a Nuclease (ThermoFisher), denatured for 10mins at 68°C and resolved by SDS-Page electrophoresis, transferred to nitrocellulose membranes, blocked in 5% milk or BSA and 0.1 % Tween for 30mins and probed. For secondary antibodies, HRP-linked anti-rabbit or mouse (Amersham) was used, and the HPR signal was visualized with SuperSignal ECL substrate (Pierce) as per the manufacturer's instructions. In all western blots, γ-tubulin (γ-TUB) serves as the loading control.

siRNA Transfections.—For siRNA knockdown the *On-Target Plus (OTP)* siRNA Smartpools from Dharmacon (GE) were used, unless otherwise indicated (see Supplementary Table S1). To deplete endogenous RAD51AP1 for rescue experiments and SIM imaging a single siRNA targeting the 3'UTR of RAD51AP1 mRNA (see Supplementary Table S1) synthesized and purchased from Dharmacon (GE). Briefly, 200,000 and 700,000 cells were seeded per well of a 6-well plate and 10cm dish containing growth medium without antibiotics, respectively. ~2hrs later cells were transfected. siRNAs and Dharmafect were diluted in OptiMEM (Life Technologies). A working siRNA concentration of 50nM was used. We used 2.5μL and 5μL Dharmafect transfection reagent per well and 10cm plate, respectively. Transfection medium was replaced with complete

culture media 24hrs later or cells were split for desired application and harvested at 72hrs post transfection, unless otherwise indicated.

Direct Immunofluorescence.—Cells on glass coverslips were washed twice in PBS and fixed with 2% PFA for 10mins. Cells were permeabilized with 0.1% (w/v) sodium citrate and 0.1 % (v/v) Triton X-100 for 5mins and incubated with fresh blocking solution (1 mg/mL BSA, 10% normal goat serum, 0.1% Tween) for at least 30mins. Primary antibodies were diluted in blocking solution and added to cells for 1hr at RT or overnight at 4°C. Next, cells were washed 3 times with PBS for 5mins and incubated with Alexa coupled secondary antibodies (488nm, 568nm, 647nm) (Life Technologies) for 1hr at RT. Then, cells were washed 3 times with PBS and mounted on slides with Prolong Gold Anti-fade reagent with DAPI (Life Technologies). Once the Prolong Antifade has polymerized and cured for ~24hrs cells were visualized by conventional florescence with 40X and/or 63X Plan λ objective (1.4 oil) using a Nikon 90i or Nikon A1R Spectral confocal microscope. For BrdU staining, U2OS cells expressing GFP-tagged RAD51AP1 and Flag-tagged TRF1-FokI were pulsed with 100μM BrdU for 2hrs before fixation with 2% paraformaldehyde for 10min. After permeabilization, cells were denatured with 500 U/mL Nuclease (Thermo Scientific) in reaction buffer (20mM Tris-HCl (pH 8.4), 2mM MgCl2, 50mM KCl in PBST) for 25min at 37°C in a humidified chamber. Coverslips were then washed in PBS1X and incubated with anti-BrdU (BD) and anti-FLAG (Sigma) antibodies for 30min at 37°C followed by 1hr secondary antibodies. For LC3 puncta detection at autophagosomes and/or autolysosomes, control and RAD51AP1 KO U2OS and VA13 clones were transfected with mCherry-GFP-LC3II expression plasmid (N'Diaye et al., 2009). After 48hrs, coverslips were fixed, washed three times in PBS and processed for IF to detect autophagosomes (co-localizations between mCherry and GFP signals) and autolysosomes (measured only by mCherry staining due to degradation of GFP signal within the acidic lysosomal compartment). For IF and western blots, cells were treated with Bafilomycin A1 (Invivogen) at 100nM for 12hrs, or Etoposide at 25 μM for 12hrs.

Immunofluorescence with fluorescent in situ hybridization (IF-FISH).—After secondary antibody incubation, cells were washed as above but then the IF staining was fixed with 2% paraformaldehyde (PFA) for 10mins. PFA was washed off with PBS and coverslips dehydrated with successive washes in 70%, 95% and 100% EtOH for 3mins, allowed to air dry completely. Next, the coverslips were mounted on glass slides with 15μl per coverslip of hybridization mix (70 % deionized Formamide, 1mg/ml of Blocking Reagent [Roche], 10mM Tris-HCl pH 7.4) containing Alexa 488-$(CCCTAA)_4$ PNA probe. DNA was denatured by setting the slides on a heating block set to 72°C for 10mins and then incubating for at least 4hrs or overnight at RT in the dark. The coverslips were then washed twice for 15mins with Wash Solution A (70% deionized formamide and 10mM Tris-HCl pH7.2) and three times with Solution B (0.1M Tris-HCl pH7.2, 0.15M NaCl and 0.08% Tween) for 5mins at RT. EtOH dehydration was repeated as above and finally the samples were mounted and analyzed as mentioned above.

Chromosome Orientation FISH (CO-FISH).—CO-FISH was performed as described (O'Sullivan et al., 2014) with the variation that cells were incubated with BrdU and BrdC

simultaneously for ~12hrs, and hybridization was performed with Alexa 488-$(CCCTAA)_4$ and Alexa 568-$(TTAGGG)_4$ PNA probes. In brief, cell cultures were incubated with 7.5mM BrdU and 2.5mM BrdC for ~12hrs. After removal of nucleotide analogs, colcemid (Gibco) was added for ~2hrs, cells were harvested by trypsinization, swelled in 75mM KCl and fixed in 70% Methanol: 30% Acetic Acid. Samples are stored at −20°C for days. Metaphase chromosomes were spread by dropping onto washed slides, then RNase A (0.5 mg/ml) and pepsin treated. Slides were incubated in 2×SSC containing 0.5 mg/ml Hoechst 33258 for 15mins in the dark and irradiated for 40mins (5.4×10^5 J/m2, energy 5400) at in a UV Stratalinker 2400 (Stratagene). The nicked BrdU/C substituted DNA strands are degraded by Exonuclease III digestion. The slides were then washed in PBS, dehydrated by EtOH washes and allowed to air dry completely. The remaining strands were hybridized with fluorescence labeled DNA probes of different colors, specific either for the positive telomere strand $(TTAGGG)_4$ (polymerized by lagging strand synthesis) (Alexa-488, green color), or the negative telomere strand $(CCCTAA)_4$, (polymerized by leading strand synthesis) (Alexa-568, red color). Prior to hybridization of the first PNA, DNA is denatured by heating at 72°C for 10mins, as in IF-FISH, and then incubated for 2hrs at RT. Slides were washed for 15mins with Wash Solution A (see IF-FISH), dried and then incubated with the second PNA for 2hrs at RT. The slides were then washed again twice for 15mins with Wash Solution A and 3 times with Wash Solution B (see IF-FISH) for 5mins at RT. The second wash contained DAPI (0.5μg/mL). Finally, cells were dehydrated in EtOH as above and mounted (Vectashield). The resulting chromosomes show dual staining and allow distinction between leading and lagging strands. Metaphase chromosomes were visualized by conventional florescence microscope with a 63X Plan λ objective (1.4 oil) on a Nikon 90i microscope.

Live Cell Imaging of Telomere Motion.—As previously (Crabbe et al., 2012), a surrogate for telomeres eGFP-TRF1 foci were tracked in a 3 dimensional volume after imaging with a Nikon A1RS point scanning confocal microscope. Fields were imaged with a 60× 1.40 NA objective using 405nm and 488nm excitation laser lines at 500nm steps in Z. Nuclear volumes were corrected for gross displacement in X & Y due to cell migration using NIS Elements software. Images were deconvolved again using NIS Elements to account warping due to spherical aberration. The nuclear volumes and relative foci positions were then corrected for nuclear rotation by defining the medial axis of a z-projected nucleus, and determining its angular displacement relative to the field. The volumetric data was rotated to correct for angular displacement relative to the previous time point. Telomere (eGFP-TRF1) foci positioning and tracks were defined with *Imaris* analysis software. Fine X, Y, and Z-axial displacement were corrected by defining a centroid point for each nuclear volume and correcting individual foci positions. Each telomere focus position was corrected relative to the centroid displacement from the previous time point in the X, Y and Z-axis. This fine correction accounts for slight nuclear drift concentrated in the Z-axis, as slight upward and downward motion of the nucleus can drastically skew the displacement of individual telomere foci. Telomere movement from a minimum of 30 cells per condition was captured and the complete motion of >100 telomeres over 60 mins analyzed using the methods previously described (Cho et al., 2014), with the adjustments for motion in z.

Telomeres whose motion could not be tracked for a complete hour were omitted from analysis.

A Euclidian model was used to calculate the vector displacement for the nuclear centroid and telomere foci over time.

$$d_{t_n} = \sqrt{\left(x_{t_n} - x_{t_{n-1}}\right)^2 + \left(y_{t_n} - y_{t_{n-1}}\right)^2 + \left(z_{t_n} - z_{t_{n-1}}\right)^2}.$$

The same vector displacement model was used in determining the mean squared displacement for foci over time.

Displacement from previous position

$$d_{t_n} = \sqrt{\left(x_{t_n} - x_{t_{n-1}}\right)^2 + \left(y_{t_n} - y_{t_{n-1}}\right)^2 + \left(z_{t_n} - z_{t_{n-1}}\right)^2}.$$

OR, displacement from origin—d= displacement

t= time

i= initial

$$d_{t_n} = \sqrt{\left(x_{t_n} - x_{t_i}\right)^2 + \left(y_{t_n} - y_{t_i}\right)^2 + \left(z_{t_n} - z_{t_i}\right)^2}$$

Structured Illumination Microscopy (SIM).—Image acquisition utilizes the Nikon N-SIM microscope platform and reconstruction algorithm. The system is optimized to acquire four fluorescent channels at excitation wavelengths 405nm, 488nm, 561nm and 647 m. The system acquires the entirety of the nuclear volume sampling at Nyquist frequency in x, y, and z. Images are reconstructed in the NIS-Elements software and a threshold for positive signal is defined to generate statistics related to the structures in three dimensions.

TRF1-FokI mediated induction of telomeric DSBs.—U2OS cells were transfected with siRNAs control or against RAD51AP1 as indicated. 48hrs later, the same cells were transfected with WT-TRF1-FokI or the inactive FokI mutant D450A. 24hrs later, cells were processed for immunofluorescence using Flag and PML antibody as described above. APBs (TRF1 and PML co-localizations), telomere number and size were quantified using NIS-Elements Advanced Research software (Nikon). For recovery assays, U2OS cells were transfected with siRNAs control or against 3'UTR of RAD51AP1 as indicated. 48hrs later, cells were transfected with GFP empty, GFP-WT, K269R, ΔSIM or ΔRAD51-RAD51AP1 constructs alone or together with WT-TRF1-FokI for another 24hrs. Then, cells were processed for IF, and APBs and telomere clustering were determined as described above. For POLD3 and RAD52 detection, control and RAD51AP1 KO clones (c1-c6) were transfected with either WT-TRF1-FokI or WT-TRF1-FokI and mcherry-RAD52. 24hrs later, cells were

processed for IF to determine the number of endogenous POLD3 or mCherry-RAD52 foci at telomeres in each condition. Quantifications were performed using NIS-Elements software (Nikon).

BrdU-Immunoprecipitation.—BrdU-IP was performed as described before with minor modification (Dilley et al., 2016). Briefly, TRF1-FokI-inducible cells were induced by adding 40ng/mL Dox for ~24hrs followed by 2hrs with 4-OHT (1μM) and Shield1 ligand (1μM). Cells were pulsed with 100μM BrdU (Sigma) for 2hrs before collection. Extracted genomic DNA (gDNA) sheared by sonication into 100–300 bp fragments. Sheared gDNA was denatured for 10mins at 95°C and cooled in an ice-water bath. Denatured gDNA was incubated with 2μg anti-IgG (Sigma) or anti-BrdU antibody (BD) diluted in immunoprecipitation buffer (0.0625 % (v/v) Triton X-100 in PBS) rotating overnight at 4°C. The next day, samples were incubated with 30μl Protein A/G agarose beads (Santa Cruz) pre-bound to a bridging antibody (Active Motif) for 1h rotating at 4°C. Beads were then washed three times with immunoprecipitation buffer and once with TE buffer. Beads were then incubated twice in elution buffer (1% (w/v) SDS in TE) for 15mins at 65°C. Pooled eluates were purified with ChIP DNA Clean & Concentrator kit (Zymo). Samples were diluted into 2×SSC buffer, treated at 95°C for 5mins, and dot-blotted onto an Amersham Hybond-N+ nylon membrane (GE). The membrane was then denatured in a 0.5N NaOH/ 1.5M NaCl solution, neutralized, and ultraviolet crosslinked. The membrane was hybridized with ^{32}P-labelled (TTAGGG)4 oligonucleotides in Church Buffer overnight at 55°C. The next day, the membrane was washed four times in 2×SSC buffer and once in 2×SSC/0.5% SDS, exposed onto a phosphoimager screen (GE Healthcare), scanned and analyzed with ImageJ.

Cycloheximide and ^{35}S pulse labeling—S35-methionine metabolic labeling was conducted as described in (Takai et al., 2007)TEL+ and ALT+ cell lines grown on 6cm plates were incubated with 100pg/mL cycloheximide and collected every 2hrs for protein analysis. Protein band intensity was determined using ImageJ and γTubulin (g-TUB) was used as a loading control. Protein half-life was determined by calculating the relative RAD51AP1 to γtubulin protein levels. Half-life was also calculated by one phase decay formula in GraphPad Prism. To study protein stability by ^{35}S labelling, TEL+ (HeLa LT, MG63) and ALT+ (U2OS, VA13) cells pulsed with ^{35}S-labelled L-cysteine and L-methionine were chased with media containing the unlabeled amino acids for the indicated times before cells were harvested in 50 mM Tris-HCl (pH 7.5), 150 mM NaCl, 1% NP-40 containing protease inhibitors lysis. RAD51AP1 was immunoprecipitated as described above, and proteins were resolved by SDS-Page electrophoresis. The protein gel was fixed in a mix of isopropanol:water:acetic acid (25:65:10) for 30min, washed in water and dried at 60°C for 1hour. The RAD51AP1 fraction remaining was detected after exposure onto a phosphoimager screen (GE Healthcare) and analyzed with ImageJ.

Flow Cytometry—Control and RAD51AP1 KO clones (c1-c6) cells were infected with lentivirus expressing shRNAs control or targeting ATG5, ATG7, ULK1 or cGAS. After two days of infection, culture media was replaced and cells were collected after another 5 days for flow cytometer analysis of Caspase 3 activation. Briefly, 1×10^6 cells were collected and

fixed in 4% PFA for 15 minutes at 4°C, washed twice in PBS and permeabilized at RT using 0.1% Triton X-100 in PBS. Then, cells were incubated with Caspase3-Alexa fluor 488 diluted in PBS overnight at 4°C. Next day, cells were washed twice in PBS and green fluorescence was analyzed by flow cytometry (Acuuri C6, BD).

Quantification and Statistical Analysis—The number of events quantified is reported in figures and figure legends. No methods were used to predetermine sample size and the investigators were not blinded to allocation during experiments and outcome assessment. GraphPad Prism 8 analytical software was used to generate graphs and to perform statistical analysis. Statistical values (p) were obtained using Student's t test or ANOVA tests. Multiple comparisons were also conducted such as when comparing data from multiple RAD51AP1 KOs to control or reference samples. Differences were considered statistically significant when *p< 0.05, **p<0.01, ***p<0.001, ****p<0.0001. Absence of statistical annotation is indicated by *ns.*

Supplementary Material

Refer to Web version on PubMed Central for supplementary material.

ACKNOWLEDGEMENTS

We are grateful to Jan Karlseder, Roger Greenberg, Patrick Ryan Potts and Titia De Lange for sharing reagents and helpful discussion of the study. This work was supported with funding from St. Baldrick's Foundation and American Cancer Society (RSG-18-038-01-DMC) to R.J.O. Work in R.J.O laboratory is supported by grant 5R01CA207209-02 from the NCI and funding from the School of Medicine at University of Pittsburgh. K.A.B is supported by grant R01ES024872 and American Cancer Society grant 129182-RSG-16-043-01-DMC. This project used the UPMC Hillman Cancer Center Flow Cytometry facility that is supported in part by award P30CA047904 and the Center for Biological Imaging (CBI) that is supported in part by the grant 1S10OD019973-O1 (to S.C.W)

REFERENCES

Banani SF, Rice AM, Peeples WB, Lin Y, Jain S, Parker R, Rosen MK, 2016 Compositional Control of Phase-Separated Cellular Bodies. Cell 166, 651–663. doi:10.1016/j.cell.2016.06.010 [PubMed: 27374333]

Bhowmick R, Minocherhomji S, Hickson ID, 2016 RAD52 Facilitates Mitotic DNA Synthesis Following Replication Stress. Mol. Cell 64, 1117–1126. doi:10.1016/j.molcel.2016.10.037 [PubMed: 27984745]

Bryan TM, Englezou A, Dalla-Pozza L, Dunham MA, Reddel RR, 1997 Evidence for an alternative mechanism for maintaining telomere length in human tumors and tumor-derived cell lines. Nat. Med. 3, 1271–1274. [PubMed: 9359704]

Cesare AJ, Kaul Z, Cohen SB, Napier CE, Pickett HA, Neumann AA, Reddel RR, 2009 Spontaneous occurrence of telomeric DNA damage response in the absence of chromosome fusions. Nat. Struct. Mol. Biol. 16, 1244–1251. doi:10.1038/nsmb.1725 [PubMed: 19935685]

Chandramouly G, McDevitt S, Sullivan K, Kent T, Luz A, Glickman JF, Andrake M, Skorski T, Pomerantz RT, 2015 Small-Molecule Disruption of RAD52 Rings as a Mechanism for Precision Medicine in BRCA-Deficient Cancers. Chem. Biol. 22, 1491–1504. doi:10.1016/j.chembiol.2015.10.003 [PubMed: 26548611]

Chen Y-A, Shen Y-L, Hsia H-Y, Tiang Y-P, Sung T-L, Chen L-Y, 2017 Extrachromosomal telomere repeat DNA is linked to ALT development via cGAS-STING DNA sensing pathway. Nat. Struct. Mol. Biol. 24, 1124–. doi:10.1038/nsmb.3498 [PubMed: 29106411]

Cho NW, Dilley RL, Lampson MA, Greenberg RA, 2014 Interchromosomal homology searches drive directional ALT telomere movement and synapsis. Cell 159, 108–121. doi:10.1016/j.cell.2014.08.030 [PubMed: 25259924]

Cukras S, Lee E, Palumbo E, Benavidez P, Moldovan G-L, Kee Y, 2016 The USP1-UAF1 complex interacts with RAD51AP1 to promote homologous recombination repair. Cell Cycle 15, 2636–2646. doi:10.1080/15384101.2016.1209613 [PubMed: 27463890]

Crabbe L, Cesare AJ, Kasuboski JM, Fitzpatrick JAJ, Karlseder J, 2012 Human telomeres are tethered to the nuclear envelope during postmitotic nuclear assembly. Cell Rep 2, 1521–1529. doi:10.1016/j.celrep.2012.11.019 [PubMed: 23260663]

Dilley RL, Verma P, Cho NW, Winters HD, Wondisford AR, Greenberg RA, 2016 Break-induced telomere synthesis underlies alternative telomere maintenance. Nature 539, 54–. doi:10.1038/nature20099 [PubMed: 27760120]

Dou Z, Xu C, Donahue G, Shimi T, Pan J-A, Zhu J, Ivanov A, Capell BC, Drake AM, Shah PP, Catanzaro JM, Ricketts MD, Lamark T, Adam SA, Marmorstein R, Zong W-X, Johansen T, Goldman RD, Adams PD, Berger SL, 2015 Autophagy mediates degradation of nuclear lamina. Nature 527, 105–109. doi:10.1038/nature15548 [PubMed: 26524528]

Dunham MA, Neumann AA, Fasching CL, Reddel RR, 2000 Telomere maintenance by recombination in human cells. Nat. Genet. 26, 447–450. doi:10.1038/82586 [PubMed: 11101843]

Egan DF, Chun MGH, Vamos M, Zou H, Rong J, Miller CJ, Lou HJ, Raveendra-Panickar D, Yang C-C, Sheffler DJ, Teriete P, Asara JM, Turk BE, Cosford NDP, Shaw RJ, 2015 Small Molecule Inhibition of the Autophagy Kinase ULK1 and Identification of ULK1 Substrates. Mol. Cell 59, 285–297. doi:10.1016/j.molcel.2015.05.031 [PubMed: 26118643]

Egan DF, Shackelford DB, Mihaylova MM, Gelino S, Kohnz RA, Mair W, Vasquez DS, Joshi A, Gwinn DM, Taylor R, Asara JM, Fitzpatrick J, Dillin A, Viollet B, Kundu M, Hansen M, Shaw RJ, 2011 Phosphorylation of ULK1 (hATG1) by AMPactivated protein kinase connects energy sensing to mitophagy. Science 331, 456–461. doi:10.1126/science.1196371 [PubMed: 21205641]

Galanty Y, Belotserkovskaya R, Coates J, Polo S, Miller KM, Jackson SP, 2009 Mammalian SUMO E3-ligases PIAS1 and PIAS4 promote responses to DNA double-strand breaks. Nature 462, 935–U132. doi:10.1038/nature08657 [PubMed: 20016603]

Garcia-Exposito L, Bournique E, Bergoglio V, Bose A, Barroso-González J, Zhang S, Roncaioli JL, Lee M, Wallace CT, Watkins SC, Opresko PL, Hoffmann J-S, O'Sullivan RJ, 2016 Proteomic Profiling Reveals a Specific Role for Translesion DNA Polymerase η in the Alternative Lengthening of Telomeres. Cell Rep 17, 1858–1871. doi:10.1016/j.celrep.2016.10.048 [PubMed: 27829156]

Gareau JR, Lima CD, 2010 The SUMO pathway: emerging mechanisms that shape specificity, conjugation and recognition. Nat. Rev. Mol. Cell Biol. 11, 861–871. doi:10.1038/nrm3011 [PubMed: 21102611]

Geiss-Friedlander R, Melchior F, 2007 Concepts in sumoylation: a decade on. Nat. Rev. Mol. Cell Biol. 8, 947–956. doi:10.1038/nrm2293 [PubMed: 18000527]

Guervilly J-H, Takedachi A, Naim V, Scaglione S, Chawhan C, Lovera Y, Despras E, Kuraoka I, Kannouche P, Rosselli F, Gaillard P-HL, 2015 The SLX4 complex is a SUMO E3 ligase that impacts on replication stress outcome and genome stability. Mol. Cell 57, 123–137. doi:10.1016/j.molcel.2014.11.014 [PubMed: 25533188]

Gui X, Yang H, Li T, Tan X, Shi P, Li M, Du F, Chen ZJ, 2019 Autophagy induction via STING trafficking is a primordial function of the cGAS pathway. Nature 567, 262–266. doi:10.1038/s41586-019-1006-9 [PubMed: 30842662]

Harding SM, Benci JL, Irianto J, Discher DE, Minn AJ, Greenberg RA, 2017 Mitotic progression following DNA damage enables pattern recognition within micronuclei. Nature 548, 466–470. doi:10.1038/nature23470 [PubMed: 28759889]

Heaphy CM, de Wilde RF, Jiao Y, Klein AP, Edil BH, Shi C, Bettegowda C, Rodriguez FJ, Eberhart CG, Hebbar S, Offerhaus GJ, McLendon R, Rasheed BA, He Y, Yan H, Bigner DD, Oba-Shinjo SM, Marie SKN, Riggins GJ, Kinzler KW, Vogelstein B, Hruban RH, Maitra A, Papadopoulos N, Meeker AK, 2011 Altered telomeres in tumors with ATRX and DAXX mutations. 333, 425–425. doi:10.1126/science.1207313

Hendriks IA, Lyon D, Young C, Jensen LJ, Vertegaal ACO, Nielsen ML, 2017 Sitespecific mapping of the human SUMO proteome reveals co-modification with phosphorylation. Nat. Struct. Mol. Biol. 24, 325–336. doi:10.1038/nsmb.3366 [PubMed: 28112733]

Henson JD, Cao Y, Huschtscha LI, Chang AC, Au AYM, Pickett HA, Reddel RR, 2009 DNA C-circles are specific and quantifiable markers of alternative-lengthening-oftelomeres activity. Nat. Biotechnol. 27, 1181–1185. doi:10.1038/nbt.1587 [PubMed: 19935656]

Hewitt G, Korolchuk VI, 2017 Repair, Reuse, Recycle: The Expanding Role of Autophagy in Genome Maintenance. Trends Cell Biol. 27, 340–351. doi:10.1016/j.tcb.2016.11.011 [PubMed: 28011061]

Jackson SP, Durocher D, 2013 Regulation of DNA Damage Responses by Ubiquitin and SUMO. Mol. Cell 49, 795–807. doi:10.1016/j.molcel.2013.01.017 [PubMed: 23416108]

Kamitani T, Kito K, Nguyen HP, Yeh ET, 1997 Characterization of NEDD8, a developmentally down-regulated ubiquitin-like protein. J. Biol. Chem. 272, 28557–28562. [PubMed: 9353319]

Karanam K, Kafri R, Loewer A, Lahav G, 2012 Quantitative live cell imaging reveals a gradual shift between DNA repair mechanisms and a maximal use of HR in mid S phase. Mol. Cell 47, 320–329. doi:10.1016/j.molcel.2012.05.052 [PubMed: 22841003]

Kim NW, Piatyszek MA, Prowse KR, Harley CB, West MD, Ho PL, Coviello GM, Wright WE, Weinrich SL, Shay JW, 1994 Specific association of human telomerase activity with immortal cells and cancer. 266, 2011–2015.

Konno H, Konno K, Barber GN, 2013 Cyclic Dinucleotides Trigger ULK1 (ATG1) Phosphorylation of STING to Prevent Sustained Innate Immune Signaling. Cell 155, 688–698. doi:10.1016/j.cell.2013.09.049 [PubMed: 24119841]

Lamoliatte F, McManus FP, Maarifi G, Chelbi-Alix MK, Thibault P, 2017 Uncovering the SUMOylation and ubiquitylation crosstalk in human cells using sequential peptide immunopurification. Nat Commun 8, 14109. doi:10.1038/ncomms14109 [PubMed: 28098164]

Levine B, Kroemer G, 2019 Biological Functions of Autophagy Genes: A Disease Perspective. Cell 176, 11–42. doi:10.1016/j.cell.2018.09.048 [PubMed: 30633901]

Liang F, Longerich S, Miller AS, Tang C, Buzovetsky O, Xiong Y, Maranon DG, Wiese C, Kupfer GM, Sung P, 2016 Promotion of RAD51-Mediated Homologous DNA Pairing by the RAD51AP1-UAF1 Complex. Cell Rep 15, 2118–2126. doi:10.1016/j.celrep.2016.05.007 [PubMed: 27239033]

Liang Q, Seo GJ, Choi YJ, Kwak M-J, Ge J, Rodgers MA, Shi M, Leslie BJ, Hopfner K-P, Ha T, Oh B-H, Jung JU, 2014 Crosstalk between the cGAS DNA Sensor and Beclin-1 Autophagy Protein Shapes Innate Antimicrobial Immune Responses. Cell Host Microbe 15, 228–238. doi:10.1016/j.chom.2014.01.009 [PubMed: 24528868]

Mackenzie KJ, Carroll P, Martin C-A, Murina O, Fluteau A, Impson DJS, Olova N, Sutcliffe H, Rainger JK, Leitch A, Osborn RT, Wheeler AP, Nowotny M, Gilbert N, Chandra T, Reijns MAM, Jackson AP, 2017 cGAS surveillance of micronuclei links genome instability to innate immunity. Nature 548, 461–. doi:10.1038/nature23449 [PubMed: 28738408]

Min J, Wright WE, Shay JW, 2017 Alternative Lengthening of Telomeres Mediated by Mitotic DNA Synthesis Engages Break-Induced Replication Processes. Mol. Cell. Biol. 37. doi:10.1128/MCB.00226-17

Modesti M, Budzowska M, Baldeyron C, Demmers JAA, Ghirlando R, Kanaar R, 2007 RAD51AP1 is a structure-specific DNA binding protein that stimulates joint molecule formation during RAD51-mediated homologous recombination. Mol. Cell 28, 468–481. doi:10.1016/j.molcel.2007.08.025 [PubMed: 17996710]

N'Diaye E-N, Kajihara KK, Hsieh I, Morisaki H, Debnath J, Brown EJ, 2009 PLIC proteins or ubiquilins regulate autophagy-dependent cell survival during nutrient starvation. EMBO Rep. 10, 173–179. doi:10.1038/embor.2008.238 [PubMed: 19148225]

Nassour J, Radford R, Correia A, Fuste JM, Schoell B, Jauch A, Shaw RJ, Karlseder J, 2019 Autophagic cell death restricts chromosomal instability during replicative crisis. Nature 565, 659–. doi:10.1038/s41586-019-0885-0 [PubMed: 30675059]

N'Diaye E-N, Kajihara KK, Hsieh I, Morisaki H, Debnath J, Brown EJ, 2009 PLIC proteins or ubiquilins regulate autophagy-dependent cell survival during nutrient starvation. EMBO Rep. 10, 173–179. doi:10.1038/embor.2008.238 [PubMed: 19148225]

O'Sullivan RJ, Arnoult N, Lackner DH, Oganesian L, Haggblom C, Corpet A, Almouzni G, Karlseder J, 2014 Rapid induction of alternative lengthening of telomeres by depletion of the histone chaperone ASF1. Nat. Struct. Mol. Biol. 21, 167–174. doi:10.1038/nsmb.2754 [PubMed: 24413054]

Özer Ö, Bhowmick R, Liu Y, Hickson ID, 2018 Human cancer cells utilize mitotic DNA synthesis to resist replication stress at telomeres regardless of their telomere maintenance mechanism. Oncotarget 9, 15836–15846. doi:10.18632/oncotarget.24745 [PubMed: 29662610]

Potts PR, Yu H, 2005 Human MMS21/NSE2 is a SUMO ligase required for DNA repair. Mol. Cell. Biol. 25, 7021–7032. doi:10.1128/MCB.25.16.7021-7032.2005 [PubMed: 16055714]

Potts PR, Yu H, 2007 The SMC5/6 complex maintains telomere length in ALT cancer cells through SUMOylation of telomere-binding proteins. Nat. Struct. Mol. Biol. 14, 581–590. doi:10.1038/nsmb1259 [PubMed: 17589526]

Psakhye I, Jentsch S, 2012 Protein Group Modification and Synergy in the SUMO Pathway as Exemplified in DNA Repair. Cell 151, 807–820. doi:10.1016/j.cell.2012.10.021 [PubMed: 23122649]

Rello-Varona S, Lissa D, Shen S, Niso-Santano M, Senovilla L, Mariño G, Vitale I, Jemaá M, Harper F, Pierron G, Castedo M, Kroemer G, 2012 Autophagic removal of micronuclei. Cell Cycle 11, 170–176. doi:10.4161/cc.11.1.18564 [PubMed: 22185757]

Sanjana NE, Shalem O, Zhang F, 2014 Improved vectors and genome-wide libraries for CRISPR screening. Nat. Methods 11, 783–784. doi:10.1038/nmeth.3047 [PubMed: 25075903]

Sfeir A, Kosiyatrakul ST, Hockemeyer D, MacRae SL, Karlseder J, Schildkraut CL, de Lange T, 2009 Mammalian telomeres resemble fragile sites and require TRF1 for efficient replication. Cell 138, 90–103. doi:10.1016/j.cell.2009.06.021 [PubMed: 19596237]

Sobinoff AP, Allen JA, Neumann AA, Yang SF, Walsh ME, Henson JD, Reddel RR, Pickett HA, 2017 BLM and SLX4 play opposing roles in recombination-dependent replication at human telomeres. EMBO J. 36, 2907–2919. doi:10.15252/embj.201796889 [PubMed: 28877996]

Sotiriou SK, Kamileri I, Lugli N, Evangelou K, Da-Re C, Huber F, Padayachy L, Tardy S, Nicati NL, Barriot S, Ochs F, Lukas C, Lukas J, Gorgoulis VG, Scapozza L, Halazonetis TD, 2016 Mammalian RAD52 Functions in Break-Induced Replication Repair of Collapsed DNA Replication Forks. Mol. Cell 64, 1127–1134. doi:10.1016/j.molcel.2016.10.038 [PubMed: 27984746]

Takai H, Wang RC, Takai KK, Yang H, de Lange T, 2007 Tel2 regulates the stability of PI3K-related protein kinases. Cell 131, 1248–1259. doi:10.1016/j.cell.2007.10.052 [PubMed: 18160036]

Verma P, Dilley RL, Zhang T, Gyparaki MT, Li Y, Greenberg RA, 2019 RAD52 and SLX4 act nonepistatically to ensure telomere stability during alternative telomere lengthening. Genes Dev. 33, 221–235. doi:10.1101/gad.319723.118 [PubMed: 30692206]

Wiese C, Dray E, Groesser T, San Filippo J, Shi I, Collins DW, Tsai M-S, Williams GJ, Rydberg B, Sung P, Schild D, 2007 Promotion of homologous recombination and genomic stability by RAD51AP1 via RAD51 recombinase enhancement. Mol. Cell 28, 482–490. doi:10.1016/j.molcel.2007.08.027 [PubMed: 17996711]

Yang K, Moldovan G-L, Vinciguerra P, Murai J, Takeda S, D'Andrea AD, 2011 Regulation of the Fanconi anemia pathway by a SUMO-like delivery network. Genes Dev. 25, 1847–1858. doi:10.1101/gad.17020911 [PubMed: 21896657]

Zhang J-M, Yadav T, Ouyang J, Lan L, Zou L, 2019 Alternative Lengthening of Telomeres through Two Distinct Break-Induced Replication Pathways. Cell Rep 26, 955–968.e3. doi:10.1016/j.celrep.2018.12.102 [PubMed: 30673617]

Highlights

- Disruption of RAD51AP1 inhibits telomere homology directed repair in ALT cancer cells.
- cGAS-ULK1-ATG7 dependent autophagy is activated upon telomere dysfunction.
- RAD51AP1 is specifically stabilized and regulated by SUMOylation.

SUMMARY SENTENCE

RAD51AP1 is required for the ALT mechanism and ALT cancer cell survival

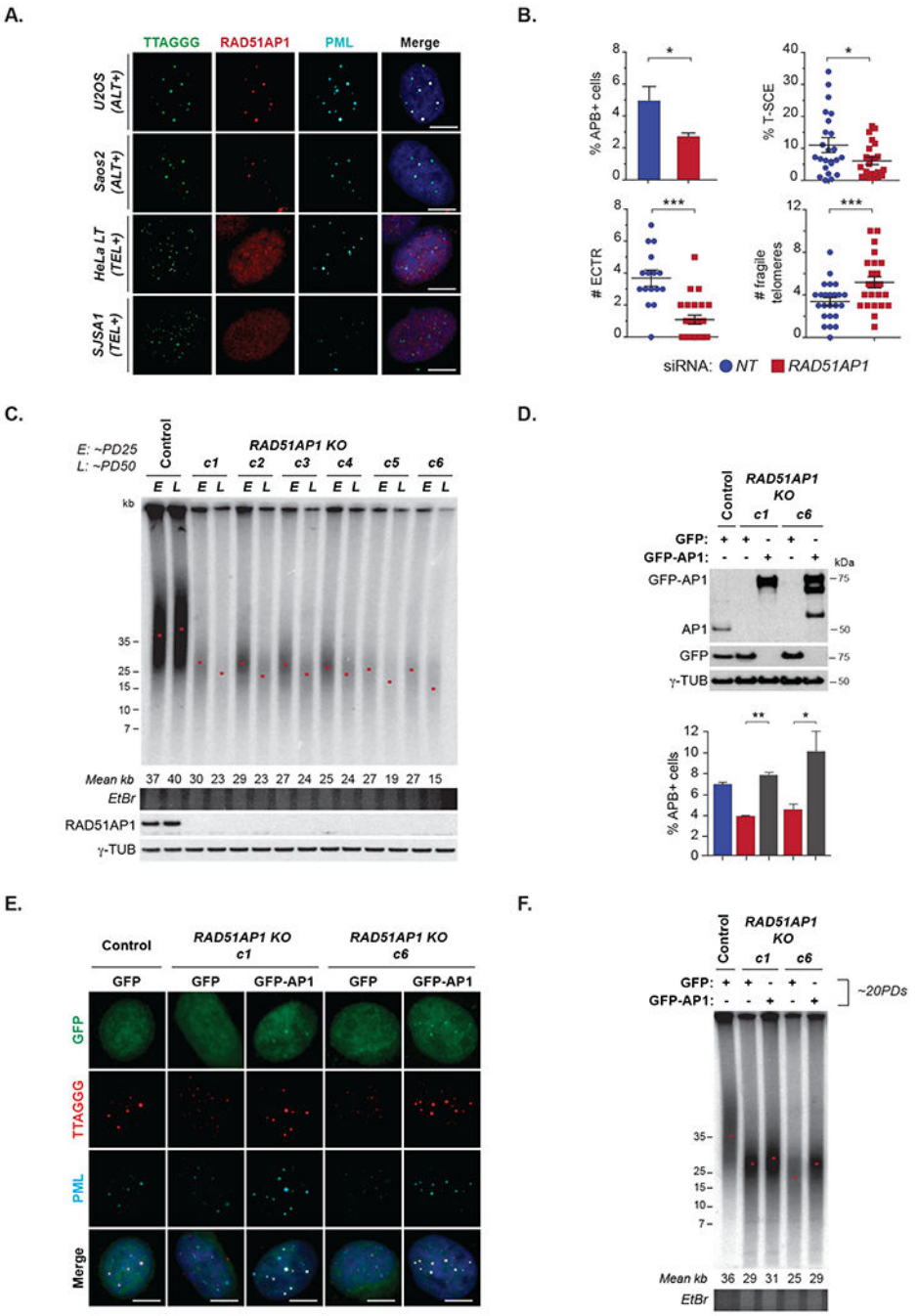

Figure 1. RAD51AP1 is required for telomere length maintenance in ALT cells.

(A) IF-FISH showing endogenous RAD51AP1 co-localization with telomeres (TTAGGG) and PML in ALT+ (U2OS, Saos2) but not in TEL+ (HeLa LT, SJSA1) cells. **(B)** Analysis of ALT phenotypes indicating percentage of ALT-associated PML Bodies (APBs), C-circles, telomeric sister chromatid exchanges (t-SCEs) and fragile telomeres in U2OS with non-targeting (NT) and RAD51AP1 siRNAs. **(C)** Telomere length analysis of control and RAD51AP1 knockout (KO) clones at early (E, ~25) and late (L, ~50) population doubling (PD) by pulsed field gel electrophoresis (PFGE). **(D)** Top: Western blot of GFP-tagged WT-

RAD51AP1 expression in RAD51AP1 KO clones. Below: Quantification of APBs percentages found in RAD51AP1 KOs expressing GFP-empty vector (EV) or GFP-WT-RAD51AP1. **(E)** Representative IF-FISH showing co-localization of GFP-WT-RAD51AP1 with telomeres and PML bodies. **(F)** PFGE of RAD51AP1 KO clones shown in (D) that were cultured for ~20PDs. Mean telomere length (kb) is indicated by the red dot. All data represents the mean +/− SEM. n=2 biological replicates. *p< 0.05, **p<0.01, ***p<0.001 (Student's t test). All scale bars, 5μm.

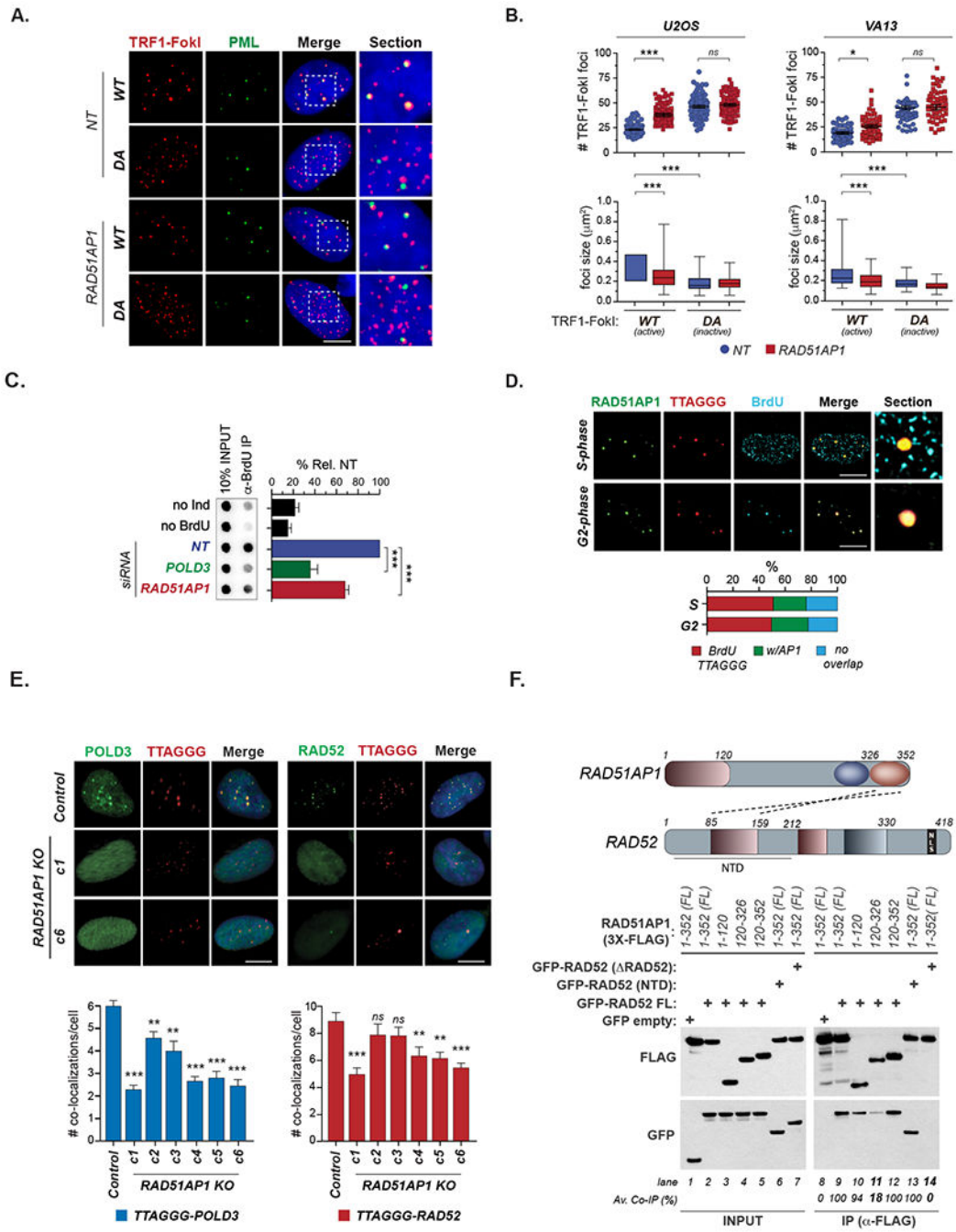

Figure 2. RAD51AP1 is a mediator of HR and BITS at ALT telomeres.

(A) IF images of TRF1-FokI-mediated telomere clustering analysis. **(B)** Graphs display the number and size of mCherry-TRF1-FokI foci observed in the indicated conditions. Data represents the mean +/− SEM. n=3 biological replicates. *p<0.05, ***p<0.001 (one-way ANOVA). **(C)** TRF1-FokI-mediated break-induced telomere synthesis assay. POLD3 knockdown was performed as a positive control. Data represents the mean +/− SEM. n=3 biological replicates. ***p<0.001 (Student's t test). **(D)** Representative structure illumination microscopy (SIM) images and graph of RAD51AP1 localization in S and G2-phase. **(E)**

Representative images and quantification of POLD3 (left) and RAD52 (right) localization at TRF1-FokI induced telomeric DSBs. Mean +/− SEM, n= 2 biological replicates **p<0.01, ***p<0.001 (Student's t test). **(F)** Top: Schematic of RAD51AP1 and RAD52 functional domains. Dotted line indicates the region in each that mediates the interaction. Below: Co-IP of GFP-RAD52 with FLAG-RAD51AP1 in U2OS cells. The average % co-IP between RAD51AP1 and RAD52 proteins is shown. n= 3 biological replicates. All scale bars, 5μm.

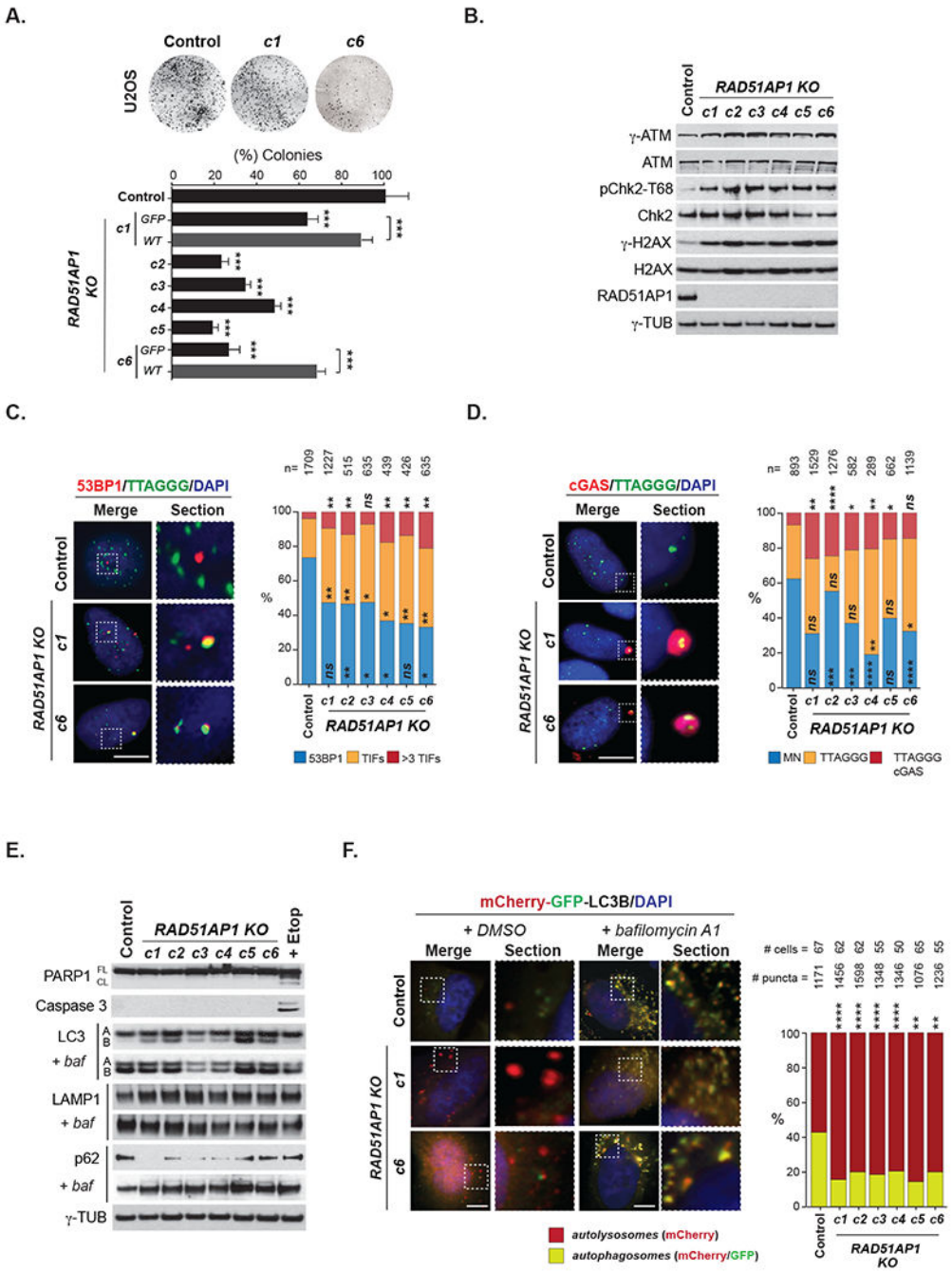

Figure 3. The fate of RAD51AP1 KO ALT+ cells.

(A) Images and quantification of colony formation assays with U2OS control and RAD51AP1 KO clones. Mean % colonies +/− SEM, n=3 biological replicates. ***p< 0.001 (Student's t test). **(B)** Western blot of phospho-ATM (S1981), phospho-Chk2 (T68) and γH2AX. **(C-D)** IF-FISH images and quantification of 53BP1 positive telomere dysfunction-induced foci (TIFs) and micronuclei containing telomeres and/or cGAS. Means +/− SEM. n=2 biological replicates. *p< 0.05, **p<0.01, ***p<0.001 (Student's t test). **(E)** Western blot of autophagy markers +/− DMSO or bafilomycin A1 (100nM for 12hrs). Cleavage of

apoptosis associated proteins PARP1 and Caspase-3 were also examined. Etoposide (25γM, 12hrs) treated U2OS cells were used as a positive control for PARP1 and Caspase-3 cleavage. **(F)** IF images and quantification of mCherry-GFP-LC3B puncta in U2OS control cells and RAD51AP1 KO clones treated with DMSO and bafilomycin A1. Data represents the mean +/− SEM. n=3 biological replicates. ****p<0.0001 (one-way ANOVA). All scale bars, 5μm.

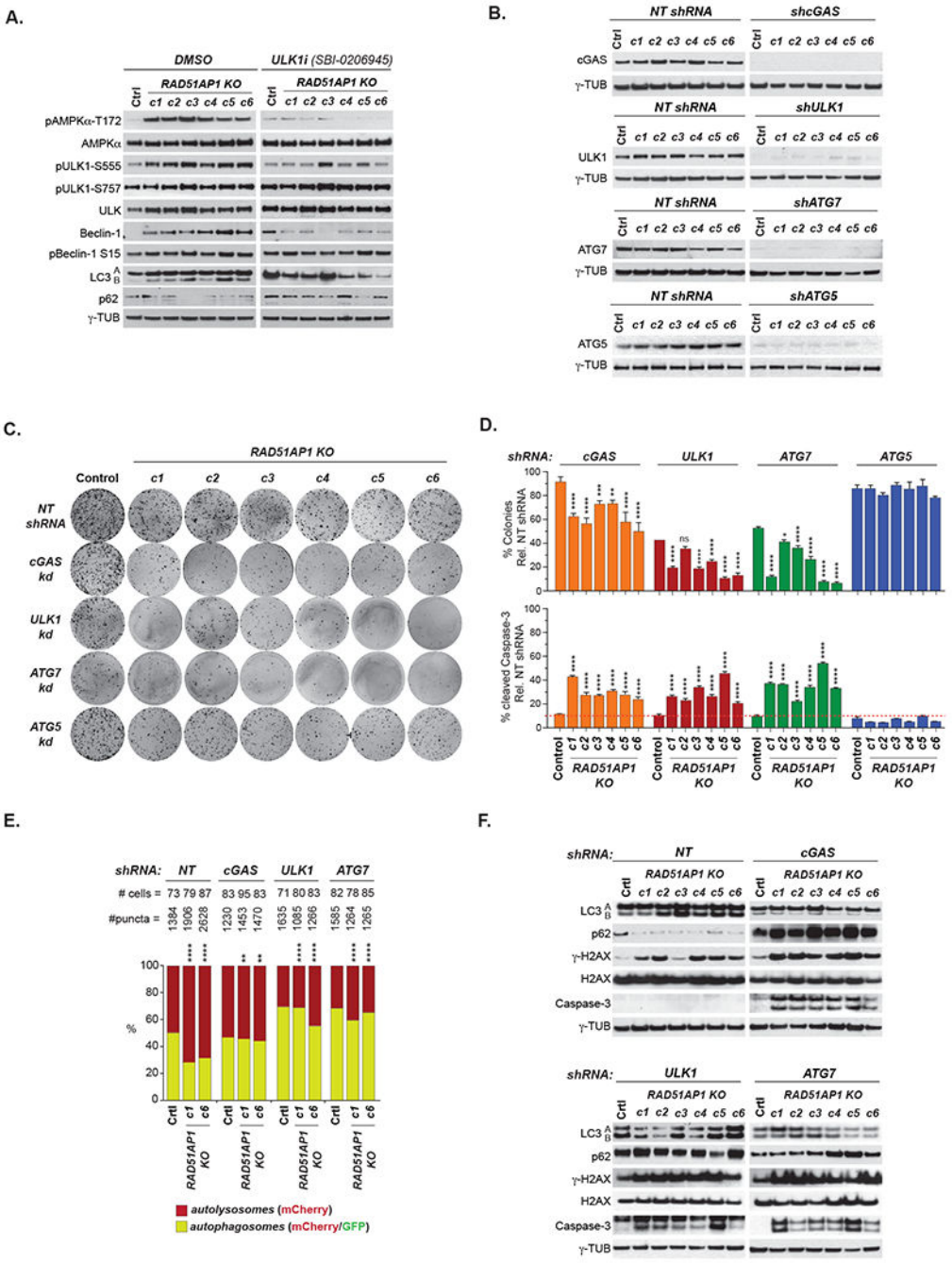

Figure 4. Activation of autophagy in RAD51AP1 KO ALT+ cells.

(A) Western blot of autophagy proteins from U2OS control and RAD51AP1 KO clones +/− DMSO or SBI-0026945 (ULK1i) (10γM, 72hrs). **(B)** Western blot of shRNA knockdown of cGAS, ULK1, ATG7 or ATG5 in U2OS control and RAD51AP1 KO clones. **(C)** Images of plates from colony formation assays with U2OS control and RAD51AP1 KO clones expressing the indicated shRNA. **(D)** Quantitation of mean % colonies and percentage of cleaved caspase-3 positive cells detected by flow cytometry from U2OS control and RAD51AP1 KO clones expressing the indicated shRNA. # colonies was normalized to % by

comparing to the corresponding clone expressing a non-targeting (NT) shRNA. Statistical significance was derived from comparisons to the control U2OS clone for each shRNA. The % cleaved caspase-3 positive cells and statistical significance was derived from comparisons to the control U2OS clone. Dotted red line indicates the mean level (%) of basal cleaved caspase-3 positive cells detected in control cells. Data represents the mean +/− SEM. n=3 biological replicates. *p< 0.05, **p<0.01, ***p<0.001, ****p<0.0001 (Student's t test). **(E)** Quantification of mCherry-GFP-LC3B puncta in control cells and RAD51AP1 KO clones expressing control (NT) or shRNAs to deplete cGAS, ULK1, ATG7 or ATG5. Data represents the mean +/− SEM. n=3 biological replicates. *p<0.01, ****p<0.0001 (one-way ANOVA). **(F)** Western blot of LC3A/B, p62, γH2AX and cleaved Caspase-3 levels in the indicated conditions.

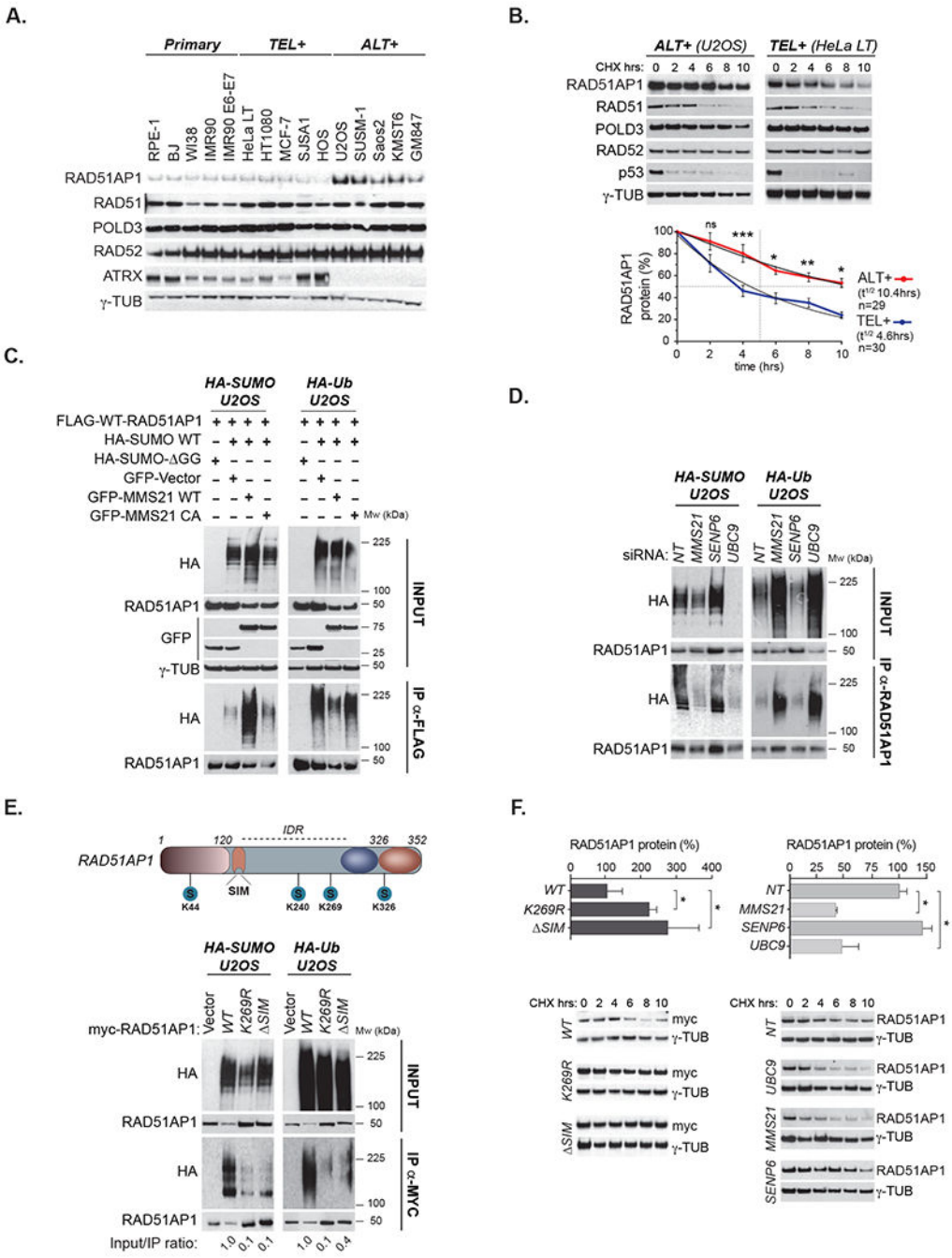

Figure 5. Stabilization of RAD51AP1 in ALT+ cells by MMS21 mediated SUMOylation

(A) Western blot of RAD51AP1, RAD51, POLD3 and RAD52 protein expression in primary, TEL+ and ALT+ cell lines. ATRX is used as a control to validate the ALT+ cell lines. **(B)** Western blots and quantification of RAD51AP1 protein levels after cycloheximide (CHX)-western analysis in ALT+ versus TEL+ cell lines. p53 was used as a positive control for CHX efficiency. Black trend line indicates RAD51AP1 turnover calculated as a function of one-phase decay. Mean RAD51AP1 protein half-life is also indicated. *p< 0.05, **p<0.01, ***p<0.001 (Student's t test). **(C)** IP-western of RAD51AP1 SUMOylation and

ubiquitination with WT or C215A GFP-MMS21 in HA-SUMO3 or HA-Ubiquitin (both WT/ΔGG)-U2OS cells. **(D)** IP-western of RAD51AP1 SUMOylation and ubiquitination after depletion of MMS21, SENP6 and UBC9. **(E)** Schematic of functional domains and consensus SUMO sites in RAD51AP1 protein and IP-western of RAD51AP1 SUMOylation and ubiquitination after expression of myc-tagged WT, K269R and ΔSIM RAD51AP1. **(F)** Western blots and quantification of RAD51AP1 protein after CHX-western in the indicated conditions. Data represents the mean +/− SEM. n=2 biological replicates. *p< 0.05 (Student's t-test).

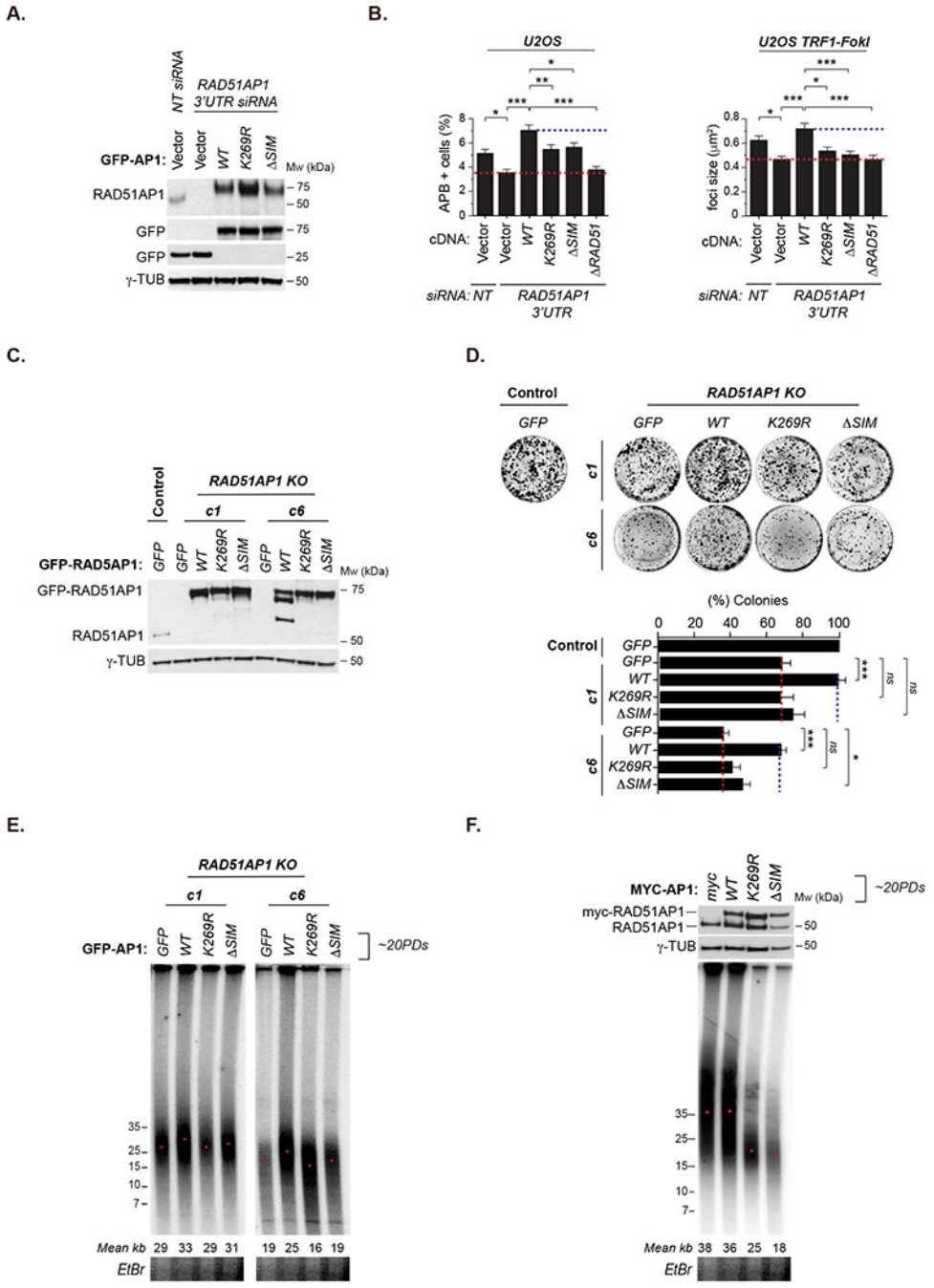

Figure 6. SUMOylation of RAD51AP1 is necessary to sustain ALT activity and telomere length.

(A) Western blots showing complementation of RAD51AP1 knockdown U2OS cells with exogenous GFP-tagged WT, K269R and ΔSIM RAD51AP1. **(B-C)** Quantification of the percentage (%) of APB positive cells and mCherry-TRF1-FokI foci size in control (NT) and RAD51AP1 depleted U2OS cells complemented with GFP-tagged WT, K269R and ΔSIM RAD51AP1. Data represents the mean +/− SEM. n=3 biological replicates. *p< 0.05, **p<0.01, ***p<0.001 (one-way ANOVA). **(D)** Top: Western blot of GFP-tagged WT, K269R and ΔSIM RAD51AP1 expression in RAD51AP1 KO clones. Below: Images and

quantification of colony formation assays with U2OS control and RAD51AP1 KO clones expressing GFP-tagged WT, K269R and ΔSIM RAD51AP1. Mean % colonies +/− SEM, n=3 biological replicates. ***p< 0.001 (Student's t test). **(E)** PFGE of RAD51AP1 KO clones expressing GFP-tagged WT, K269R, ΔSIM RAD51AP1 for ~20 PDs **(F)** Western blots and PFGE with U2OS cells stably expressing myc-tagged WT, K269R, DSIM RAD51AP1 for ~20 PDs. DNA loading is shown by section of EtBr stained DNA gel. Mean telomere length is indicated as kb and by the red dot.

KEY RESOURCES TABLE

REAGENT or RESOURCE	SOURCE	IDENTIFIER
Antibodies		
RAD51AP1	Mauro Modesti	#805 (Modesti et al., 2007)
RAD51AP1	Mauro Modesti	#806 (Modesti et al., 2007)
POLD3 (3E2)	Abnova	Cat. # H00010714-M01
ATRX (D1N2E)	Cell Signaling	Cat. # 14820
RAD52 (F7)	Santa Cruz	Cat. # sc-365341
RAD51 (H-92)	Santa Cruz	Cat. # sc-8349
FLAG (M2)	Sigma-Aldrich	Cat. # F1804
γ-TUB	Sigma-Aldrich	Cat. # T-6557
RPA2 (9H8)	Abcam	Cat. # ab2175
MMS21	Novus	Cat. # NBP2-42643
UBC9	Cell Signaling	Cat. # 4918
SENP6 (M01)	Abnova	Cat. # H00026054-M01
PML (H-238)	Santa Cruz	Cat. # sc-5621
PML (PG-M3)	Santa Cruz	Cat. # sc-966
cGAS	Cell Signaling	Cat. # 15102
γ-H2AX (Ser139)	Millipore	Cat. # 05-636
H2AX	Abcam	Cat. # ab11175
Phospho-Chk2 (Thr68)	Cell Signaling	Cat. # 2661
Chk2	Cell Signaling	Cat. # 2662
53BP1 (H-300)	Santa Cruz	Cat. # sc-22760
Cyclin B1 (D5C10)	Cell Signaling	Cat. # 12231
LC3A/B (D3U4C)	Cell Signaling	Cat. # 12741
LAMP1 (D2D11)	Cell Signaling	Cat. # 9091
SQSTM1/p62	Cell Signaling	Cat. # 5114
HA-HRP	Miltenyi BioTech	Cat. # 130-091-972
GFP-HRP	Miltenyi BioTech	Cat. # 130-091-972
Anti-Rabbit-HRP	Cell Signaling	Cat. # 7474P2
Anti-Mouse-HRP	Cell Signaling	Cat. # 7076
c-MYC (9E11)	Santa Cruz	Cat. # sc-40
BrdU (clone B44)	BD Biosciences	Cat. # 347580
PARP1	Active Motif	Cat. # 61638
Phospho-ATM (Ser1981)	Cell Signaling	Cat. # 13050
ATM	Sigma	Cat. # A1106
c-Caspase 3 (Asp175)	Cell Signaling	Cat. # 9661
c-Caspase-3 (Asp175) Alexa-488	Cell Signaling	Cat. # 9669
ATG7 (D12B11)	Cell Signaling	Cat. # 8558

REAGENT or RESOURCE	SOURCE	IDENTIFIER
ATG5 (D5F5U)	Cell Signaling	Cat. # 12994
ULK1	Cell Signaling	Cat. # 8054
ULK1 (Ser757)	Cell Signaling	Cat. # 6888
ULK1 (Ser555)	Cell Signaling	Cat. # 5869
AMPK	Cell Signaling	Cat. # 2532
AMPK (Thr172)	Cell Signaling	Cat. # 2535
Beclin-1 (D40C5)	Cell Signaling	Cat. # 3495
Phospho-Beclin-1 (Ser15) (D4B7R)	Cell Signaling	Cat. # #84966
siRNAs		
Non-targeting control	Dharmacon	D-001810-10-0020
RAD51AP1	Dharmacon	L-017166-00-0005
RAD51AP1 3’UTR	Dharmacon	auggcauaugucuccgauuua
UBC9	Dharmacon	L-004910-00-0005
MMS21	Dharmacon	L-018070-00-0005
SENP6	Dharmacon	L-006044-00-0005
POLD3	Dharmacon	L-026692-01-0005
MRE11	Dharmacon	L-009271-00-0005
CtIP	Dharmacon	L-011376-00-0005
RPA1	Dharmacon	L-015749-01-0005
RAD51	Dharmacon	L-003530-00-0005
shRNAs		
pLKO.1-puro	Addgene	Addgene plasmid # 10878
pLKO.1-puro-shRNA ATG7	Sigma	TRCN0000007586
pLKO.1-puro-shRNA ULK1	Sigma	TRCN0000342643
pLKO.1-puro-shRNA ATG5	Sigma	TRCN0000150645
pLKO.1-puro-shRNA cGAS	Sigma	TRCN0000128706
Recombinant DNA Vectors		
myc-pLPC	Titia de Lange	Addgene plasmid # 12540
EGFP-C1	Clontech	Cat. #6084-1
GFP-RAD51AP1	Mauro Modesti	(Modesti et al., 2007)
Flag-TRF1-FokI WT/D450A	Roger Greenberg	(Dilley et al., 2016)
GFP-RAD52	Richard T. Pomerantz	(Chandramouly et al., 2015)
HA-SUMO3	Edward Yeh	Addgene plasmid # 17361 (Terui et al., 2004)
HA-Ubiquitin	Edward Yeh	Addgene plasmid # 18712 (Kamitani et al., 1997)
pBABE-puro-mCherry-EGFP-LC3B	Jayanta Debnath	Addgene plasmid # 22418 (N’Diaye et al., 2009)
mCherry-RAD52	Galit Lahav	(Karanam et al., 2012).
Oligonucleotides to generate recombinant DNA vectors		
See Table S1.		
CRISPR vectors and guide RNA sequences		

REAGENT or RESOURCE	SOURCE	IDENTIFIER
Lenti-CRISPR V2	Feng Zhang	Addgene plasmid #52961 (Sanjana et al., 2014)
sgRAD51AP1 1 (Fw)	Lenti-CRISPR V2	caccgttccggagattgttcaagtt
sgRAD51AP1 1(Rv)	Lenti-CRISPR V2	aaacaacttgaacaatctccggaac
sgRAD51AP1 2 (Fw)	Lenti-CRISPR V2	caccgtcaaactgtgagtaattgac
sgRAD51AP1 2 (Rv)	Lenti-CRISPR V2	aaacgtcaattactcacagtttgac
sgRAD51AP1 3 (Fw)	Lenti-CRISPR V2	caccgtgcacattagtggtgactgt
sgRAD51AP1 3 (Rv)	Lenti-CRISPR V2	aaacacagtcaccactaatgtgcac
sgRAD51AP1 4 (Fw)	Lenti-CRISPR V2	caccgattctgatttgacggcagc
sgRAD51AP1 4 (Rv)	Lenti-CRISPR V2	aaacgctgccgtcaaatcagaatc
RAD51AP1 rescue (Fw)	Lenti-CRISPR V2	ctttatcagtgaaggaacttgcaacagtcaccactaatgtg
RAD51AP1 rescue (Rv)	Lenti-CRISPR V2	cacattagtggtgactgttgcaagttccttcactgataaag
Chemicals, peptides and transfection reagents		
SBI-0206965 (ULKi)	Cell Signaling	Cat. # 29089
AluI	New England Biolabs	Cat. # R0137
MboI	New England Biolabs	Cat. # R0137
Phi29	New England Biolabs	Cat. # M0269
Benzonase	Merck MIllipore	Cat. # 70746
4-hydroxytamoxifen	Sigma	Cat. # H7904
Doxycycline	Clontech	Cat. # 631311
Shield Ligand	Clontech	Cat. # 632189
Tel C PNA probe	PNA Bio	Cat. # F1004
Tel G PNA probe	PNA Bio	Cat. # F1006
Deposited data		
Raw images, data sheets and immunoblots	Mendeley	DOI: http://dx.doi.org/10.17632/7frzkkgz74.2